1 # High quality epitaxial graphene on 4H-SiC by face-to-face growth in Ultra

2 # High Vacuum

3 N. Zebardastan[1,2], J. Bradford[2,3], J. Lipton-Duffin[1,2], J. MacLeod[1,2], K. Ostrikov[1,2] , Massimo

4 Tomellini[4,5], Nunzio Motta[*1,2]

5 1. Centre for Materials Science, Queensland University of Technology, Brisbane 4001, QLD,

6 Australia

7 2. School of Chemistry and Physics, Queensland University of Technology, Brisbane 4001,

8 QLD, Australia

9 3. School of Physics and Astronomy, University of Nottingham, Nottingham NG7 2RD,

10 United Kingdom

11 4. Dipartimento di Scienze e Tecnologie Chimiche, Università degli Studi di Roma Tor

12 Vergata, Via della Ricerca Scientifica,00133 Rome, Italy

13 5. Istituto di Struttura della Materia, CNR, Via Fosso del Cavaliere 100,00133 Rome, Italy

14 E-mail: n.motta@qut.edu.au

15 **Abstract**

16 Epitaxial graphene on SiC is the most promising substrate for the next generation 2D

17 electronics, due to the possibility to fabricate 2D heterostructures directly on it, opening the

18 door to the use of all technological processes developed for silicon electronics. To obtain a

19 suitable material for large scale applications, it is essential to achieve perfect control of size,

20 quality, growth rate and thickness. Here we show that this control on epitaxial graphene can be

21 achieved by exploiting the Face-to-Face (FTF) annealing of SiC in Ultra High Vacuum (UHV).

[*] Corresponding author. Tel: +61731385104. E-mail: n.motta@qut.edu.au

22 With this method, Si atoms trapped in the narrow space between two SiC wafers at high
23 temperatures contribute to the reduction of the Si sublimation rate, allowing to achieve smooth
24 and virtually defect free single graphene layers. We analyse the products obtained on both on-
25 axis and off-axis 4H-SiC substrates in a wide range of temperatures (1300 - 1500°C),
26 determining the growth law with the help of X-ray Photoelectron Spectroscopy (XPS). Our
27 epitaxial graphene on SiC has terrace widths up to 10 µm (on-axis) and 500 nm (off-axis) as
28 demonstrated by Atomic Force Microscopy (AFM) and Scanning Tunnelling Microscopy
29 (STM), while XPS and Raman spectroscopy confirm high purity and crystalline quality.

30 **Keywords:** epitaxial graphene, thermal decomposition, silicon sublimation, ultrahigh
31 vacuum, face to face technique, 4H-SiC, on-axis SiC, off-axis SiC.

32 1. Introduction

33 Two-dimensional graphene was first isolated in 2003 using Scotch tape to mechanically
34 exfoliate graphene monolayers from graphite [1, 2]. This peeling technique could generate
35 graphene flakes of up to 100µm for laboratory research [3]. Mechanical and other chemical
36 exfoliation techniques proposed after graphene's isolation [4] are not suitable to large scale
37 applications in electronics, as it is not possible to achieve a perfect control of the quality of
38 graphene and of the number of layers [5-7]. Transfer of graphene to the required substrate is
39 also costly, time consuming and can cause defects and contamination at the graphene/substrate
40 interface [8-11].

41 Epitaxial graphene on SiC obtained by Si sublimation in UHV for the first time in 2004 [12],
42 remains a promising route towards graphene-based electronics as it relies on the well-
43 established semiconductor technology production chain [13]. Other techniques to obtain
44 epitaxial graphene have been demonstrated, like direct synthesis of planar graphene on Ni
45 substrate by thermal chemical vapor deposition (CVD) [14]. The morphology of the metal

46 substrates determines the quality and structure of graphene, and many techniques are used to
47 treat the surface for the production of high-quality uniform graphene layers such as annealing
48 under CH_4 or plasma treatment [15, 16]. However, the complicated process of transferring
49 graphene layer to another substrate gives origin to defects and makes these methods not suitable
50 for large scale electronics applications. Sublimation of SiC at high temperature is the most
51 justified, scalable, and simple way of producing large scale, uniform, high quality graphene on
52 a semiconducting substrate [17-19]. Graphitization of SiC by decomposition at high
53 temperature in ultrahigh vacuum was first reported in 1962 while studying the transition of the
54 surface structure of SiC at different temperatures but the number of graphene layers was
55 unknown [20]. De Heer was the first to grow epitaxial graphene on 6H-SiC by Si sublimation
56 in UHV [21, 22].

57 The growth of epitaxial graphene on semi-insulating SiC opens the way to a new generation of
58 electronics, however it is imperative to achieve a perfect control of defects, surface structure
59 and number of graphene layers [23, 24] to obtain the qualities required by the electronic
60 industry. Several studies report about the growth optimization of epitaxial graphene obtained
61 by thermal decomposition on different polytypes of SiC (6H, 4H and 3C) in ambient pressure
62 or under UHV conditions [17, 25-30]. Growth of epitaxial graphene at atmospheric pressure
63 requires high temperatures (1500-1700 ˚C) [31] which causes a high level of SiC step bunching,
64 while it can be obtained in UHV at lower temperature with a reduced step bunching [17, 32].
65 During thermal decomposition Si atoms sublimate and the remaining carbon atoms diffuse and
66 reorganize on the surface, forming the graphene honeycomb lattice [33-37]. The different
67 polytypes of SiC have different surface free energies which influence the graphene growth
68 mechanism [38, 39]. On 4H-SiC the sublimation of Si from the surface of SiC under UHV
69 starts at temperatures above 1200 ˚C and the optimum growth condition results in epitaxial
70 graphene with terraces of up to 200 nm width [40]. The slower the sublimation rate of Si, the

71 higher the quality of epitaxial graphene as the carbon atoms have enough time to rearrange and
72 form crystal domains [41, 42]. So far sublimation rate of Si is reported to be controlled by
73 techniques such as Confinement Controlled Sublimation (CCS), supplying Si vapour, flowing
74 inert gas and polymer assisted sublimation [42, 43]. These techniques are used to induce a
75 counter pressure at the surface to minimize Si sublimation and create nearly equilibrium
76 conditions for evaporating Si [27]. Although the CCS of Si for growth of epitaxial graphene is
77 not a new technique, the sublimation of Si is obtained using an induction furnace under ambient
78 or low pressure and using a graphite box to control the sublimation rate [42, 44, 45].

79 In this research, the Face-to-Face growth technique is used to obtain high quality epitaxial
80 graphene with significantly large epitaxial graphene steps (10 µm (on-axis) and 500 nm (off-
81 axis)). The Face-to-Face technique previously introduced to grow epitaxial graphene on 6H-
82 SiC under high vacuum (10^{-6} Torr) and performed the experiment in a limited range of
83 temperatures [45]. In our experiment, we extended the method to UHV (10^{-10} mBar) and used
84 both on-axis and off-axis 4H-SiC. We performed the experiment in an extended range of
85 temperatures and for different durations, providing a full account of the graphene quality and
86 thickness from 1260 ˚C to 1500 ˚C and for times variable between 5 min and 20 minutes.

87 The Face-to-Face technique provides a very simple solution to slow down the evaporation of
88 Si and effectively control the growth rate and structure of graphene with the advantage of
89 growing two samples at the same time. The growth parameters on both on-axis and off-axis
90 SiC are optimized based on the desired number of graphene layers and terrace size. We develop
91 a kinetic model to explain the time evolution of the graphene layer by comparing the intensity
92 of the C1s core level XPS spectra in SiC and graphene as a function of time and annealing
93 temperature. Our model supports the layer-by-layer growth of epitaxial graphene and allows
94 us to calculate the activation energy of the process.

95 **Experimental method**

96 *Epitaxial Graphene Synthesis*: Initially samples were cleaned under sonication in acetone,
97 ethanol, and deionized water for 20 minutes each and dried in air before mounting on the
98 sample holder. Two SiC substrates were sandwiched with the Si faces facing each other,
99 separated by two pieces of tantalum foil 25 μm thick (99.9% purity, Goodfellow). Figure 1(a)
100 illustrates the sandwich of SiC samples mounted on the direct current sample holder (Scienta
101 Omicron GmbH) under a magnifier. Samples were introduced into an ultrahigh vacuum system
102 (Scienta Omicron GmbH) and degassed overnight at 650 ˚C to remove contaminants. Epitaxial
103 graphene was grown on both on-axis and 4˚ off-axis n-type 4H-SiC(0001) wafers (CREE,
104 Double sided polish Si face CMP epi ready) using thermal decomposition (direct current
105 heating) at ≥1260 ˚C for different period of times at a base pressure of $\sim 1\times10^{-10}$ mbar (Figure
106 1(b)). An optical pyrometer with temperature uncertainty of ±10 ˚C was used to monitor the
107 temperature of the substrates (emissivity=0.95). Several growths were performed to follow the
108 evolution of the epitaxial graphene on both substrates. Figure 1(c) illustrates the mechanism of
109 growth in the FTF technique and how the Si counter pressure on the SiC surface from the
110 adjacent sample helps to control the growth rate and improves the structure of epitaxial
111 graphene steps. To prove the effectiveness of FTF growth technique, epitaxial graphene was
112 grown on both on-axis and 4˚ off-axis SiC by standard method of thermal decomposition as
113 well. In this method single SiC substrates were annealed at ≥1280 ˚C for different period of
114 times at a base pressure of $\sim 1\times10^{-10}$ mbar.

115 After removing the samples from vacuum and separating the two wafers, atomic resolution
116 imaging of the surface was obtained by mounting one of the two samples in an STM sample
117 holder and re-introducing it quickly into the vacuum. The same sample was then analysed ex-
118 situ by AFM to visualize the large-scale surface structure and by XPS the number of graphene
119 layers were calculated. The existence of epitaxial graphene and the number of graphene layers

120 were further confirmed using Raman spectroscopy. Different phases of partially FTF grown
121 epitaxial graphene were shown by Kelvin Probe Force Microscopy (KPFM). Figure 1(d) shows
122 the schematic diagram of monolayer epitaxial graphene on SiC with a buffer layer. The
123 morphology of the samples grown by standard technique were analysed in-situ by STM after
124 growth (Figure S2).

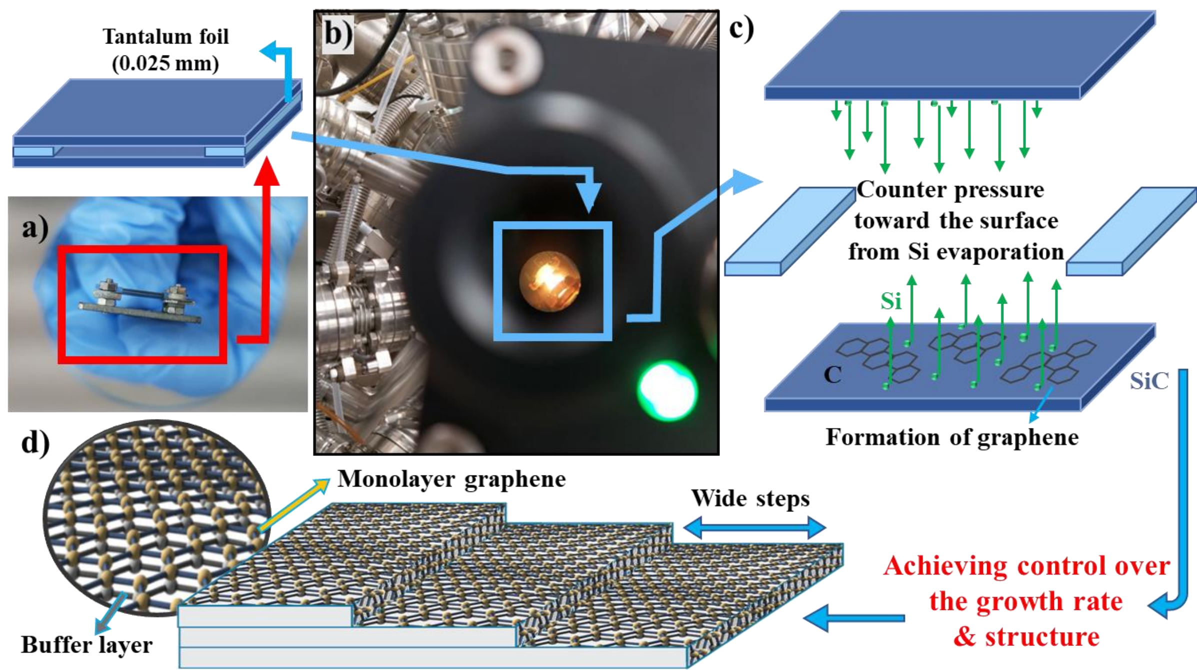

125

126 **Figure 1. Our demonstrated concept of FTF growth technique enables control over the growth rate and**
127 **structure of epitaxial graphene on SiC.** (a) The sandwich of two SiC samples mounted on the sample holder
128 for epitaxial graphene growth using the FTF technique. (b) The sample in (a) as seen through the optical
129 pyrometer while annealing at high temperature in an UHV system. (c) The schematic model of growth
130 mechanism. (d) The model of monolayer epitaxial graphene covering the SiC steps.

131 *Material Characterization*: The morphology of epitaxial graphene was studied using AFM and
132 STM. A Dimension Icon PT (Bruker) was used to acquire the AFM images at room temperature
133 using a ScanAsyst in Air probe under PeakForce tapping mode. Room temperature STM was
134 conducted in a Scienta Omicron GmbH ultrahigh vacuum system with a base pressure of ~
135 1×10^{-11} mbar using an electrochemically etched W tip. A Variable Temperature (VT-
136 AFM/XA) scanning tunnelling microscope was used to obtain the STM images at room

137 temperature. Samples were degassed at 300 ˚C for two hours by electron bombardment in
138 ultrahigh vacuum before STM. AFM and STM images were analysed using Gwyddion
139 software (http://gwyddion.net/). Kelvin Probe Force Microscopy (KPFM) measurements were
140 acquired with an Asylum Cypher-S atomic force microscope (Oxford Instruments) using Pt
141 coated Si cantilevers with a spring constant of 7 Nm-1 (SPARK70Pt, NuNano). The KPFM
142 measurement is a two-pass technique where, on the second pass, the tip is raised 3 nm above
143 the surface and retraces the surface topography with AC and DC biases applied to the tip. For
144 the data reported a 500 mV AC voltage (frequency matched to the cantilever drive frequency),
145 and a 3 V DC voltage was applied to the tip.The chemical composition of epitaxial graphene
146 was obtained ex-situ by X-ray photoelectron spectroscopy (XPS) in a Kratos Axis Supra
147 system. XPS measurements were acquired with monochromatic Al Kα radiation (1486.7 eV,
148 225W), and high-resolution core level spectra were collected at a pass energy of 20 eV whereas
149 the survey spectra were collected at 160 eV pass energy. The XPS data were analysed using
150 CasaXPS software (http://www.casaxps.com/)[46] and the binding energy of the components
151 were calibrated based on Si $2p_{3/2}$ core level in SiC at 100.6 eV. The Raman spectra were
152 collected from a Renishaw inVia Raman spectrometer with an excitation wavelength of 532
153 nm using a frequency doubled NdYAG laser with spot size of 1 µm. The laser power was kept
154 at 1% to protect the epitaxial graphene and the beam was focussed on the sample using a ×50
155 Short Working Distance (SWD) objective lens.

156 **2. Results and discussion**

157 **2.1 X-ray photoelectron spectroscopy**

158 Figure 2 a-d shows the evolution of the SiC and graphene components of the C1s XPS core
159 level spectra as a function of growth temperature (Figure 2a and 2c) and time (Figure 2b and
160 2d) for epitaxial graphene grown on both on-axis and off-axis SiC respectively. The C 1s peaks
161 include a SiC bulk component (283.7 ± 0.05 eV), sp^2 C-C bond of graphene (284.6 ± 0.05 eV)

162 and the two surface buffer layer components S1 and S2 (284.8 ± 0.05 eV and 285.4 ± 0.05 eV)
163 respectively. The S1 and S2 components with a 1:2 intensity ratio originates from the (6√3×6√3
164)R30° reconstructed layer where S1 is related to the carbon atoms partially bonded with the Si
165 atoms underneath and S2 is related to the stronger sp^2 bonded carbons within the layer [47, 48].
166 The yellow component at higher binding energy (~ 286.7 ± 0.1 eV) is assigned to CO_x. In the
167 FTF technique, the samples must be extracted from UHV and dismounted to perform the XPS
168 analysis, exposing the surface to contamination and deposition of water vapour and CO_x during
169 the transport. By increasing the annealing temperature, the relative concentration of the
170 graphene component increases as the growth of epitaxial graphene proceeds, while the SiC
171 peak decreases (Figure 2a and 2c). The same effect is obtained by increasing the growth time,
172 as expected (Figure 2b and 2d). We observed that the graphene component increase is more
173 sensitive to changes in the annealing temperature than changes in growth time.

174 The intensity ratio of the graphene component (N_G) to the SiC component as a reference peak
175 (N_R) is used to calculate the thickness of epitaxial graphene grown on on-axis and off-axis SiC
176 using the relation [49]:

177 $$\frac{N_G}{N_R} = \frac{T(E_G)\rho' C_G \Lambda'(E_G)[1-exp\,(-t/\Lambda'(E_G))]}{T(E_R)\rho' C_R \Lambda(E_R)\,exp\,(-t/\Lambda'(E_R))} \times F, \quad (1)$$

178 where T is the transmission function of the analyser, E is the kinetic energy of photoelectrons
179 for graphene (E_G) and SiC (E_R) in XPS, ρ is the atomic density of the material, C is the
180 differential cross section ($d\sigma/d\Omega$), Λ is the inelastic mean free path and F is a geometrical
181 correction factor caused by photoelectron diffraction. The superscript ′ denotes quantities that
182 apply to the graphene overlayer rather than the bulk SiC. The TPP-2M formula is used to
183 calculate the estimated inelastic mean free path of graphite and SiC [50]. By calculating the
184 thickness of epitaxial graphene t using Equation 1 and dividing this value by the graphene
185 interlayer spacing value of 3.35 Å, the number of layers for each sample is calculated. The

186 atomic concentration of graphene and SiC extracted from the C1s XPS peak, and the calculated
187 number of graphene layers at various annealing temperatures and growth times are tabulated
188 in Table 1 for on-axis and off-axis SiC. From Table 1 is apparent that the growth rate is higher
189 for off-axis SiC compared to on-axis SiC. Monolayer graphene is obtained by annealing on-
190 axis and off-axis SiC at 1350˚C and 1300˚C for 10 minutes respectively. As a comparison, the
191 atomic concentration of graphene and SiC C1s components and the calculated number of
192 graphene layers obtained with the standard growth technique are tabulated in Table S1 for both
193 on-axis and off-axis SiC. Note that in this case by annealing SiC at 1280 ˚C for just 1 minute
194 results in 3.87 and 2.69 graphene layers for on-axis and off- axis respectively. This proves the
195 effectiveness of FTF growth technique in comparison with the standard method in controlling
196 the growth rate of epitaxial graphene. The C1s XPS core level spectra of the samples tabulated
197 in table S1 are shown in Figure S1.

198 **Table 1. Calculated number of graphene layers in FTF method.** The atomic concentration of SiC and graphene
199 components of C1s XPS core level spectra and the number of graphene layers calculated accordingly for epitaxial graphene
200 grown by FTF technique at different growth temperatures and time on on-axis and off-axis SiC.

On-axis SiC						Off-axis SiC					
T (˚C)	Growth time (mins)	Atomic concentration (%)		Graphene layers	Error ±	T (˚C)	Growth time (mins)	Atomic concentration (%)		Graphene layers	Error ±
		SiC	Graphene					SiC	Graphene		
1280	15	72.82	8.83	0.31	0.09	1300	5	52.62	14.01	0.67	0.53
							10	51.65	30.24	1.37	0.10
	20	62.87	24.61	0.96	0.12		15	37.33	22.28	1.39	0.49
1300	10	70.79	19.47	0.69	0.17		20	49.34	31.37	1.48	0.12
	15	64.44	19.46	0.75	0.12	1350	5	42.27	36.14	1.89	0.13
	20	68.22	21.69	0.91	0.07		10	47.17	40.34	1.91	0.28
1350	5	63.72	20.55	0.80	0.15		15	37.81	40.42	2.27	0.42
	10	61.19	26.24	1.04	0.12		20	38.19	43.82	2.41	0.31

	15	53.51	31.23	1.37	0.30	1400	5	47.29	32.02	1.56	0.28
	20	47.28	34.87	1.67	0.15		10	33.74	44.98	2.71	0.74
1400	5	66.81	18.62	0.70	0.15		15	31.84	51.66	3.15	0.55
	10	56.14	33.01	1.37	0.08		20	29.51	51.39	3.32	0.48
	15	46.91	31.63	1.55	0.30						
1450	5	52.64	32.8	1.44	0.11						
	10	39.25	39.82	2.18	0.65						
	15	43.14	33.27	2.24	0.13						
1500	5	38.37	48.87	2.49	0.55						
	10	30.81	49.99	3.15	0.62						

201

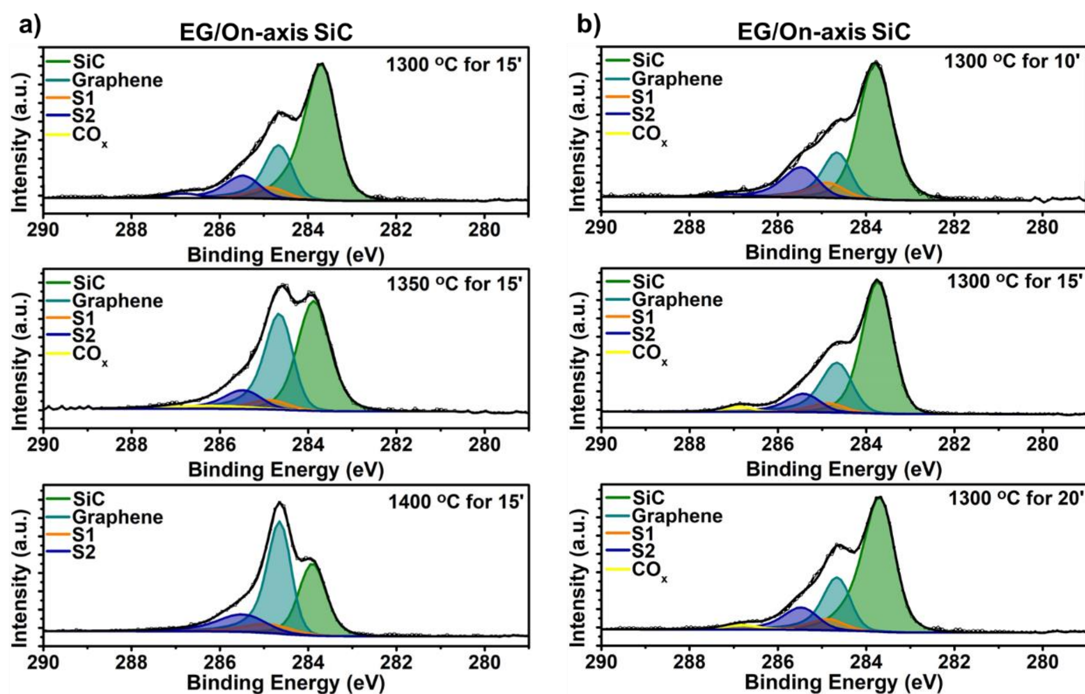

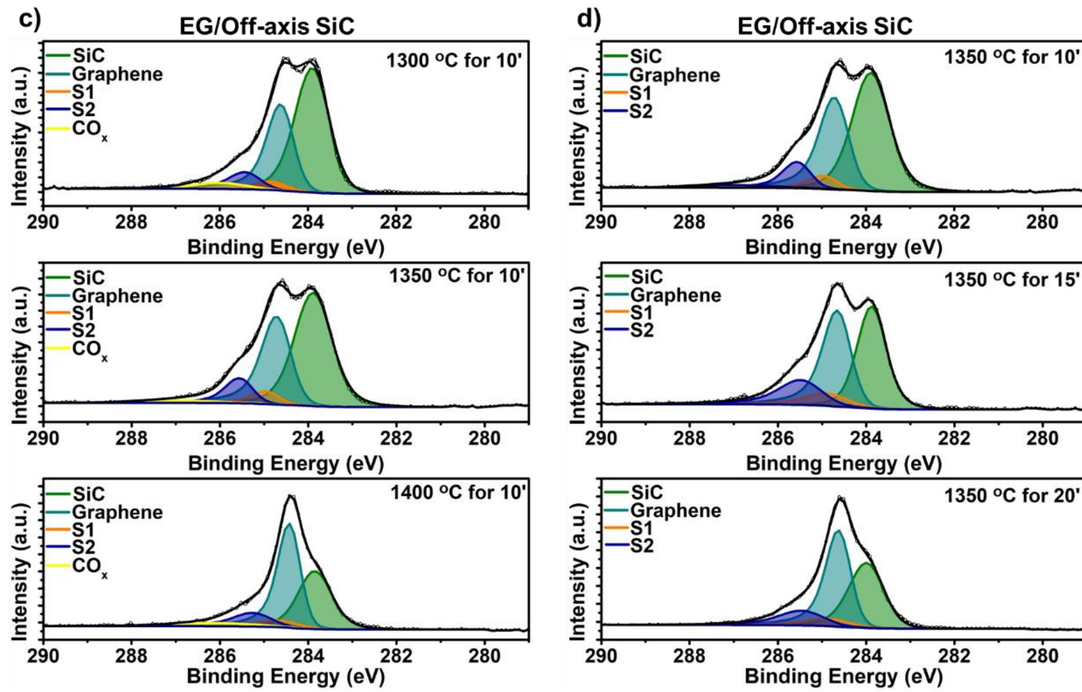

202 **Figure 2.Chemical characterization of FTF grown epitaxial graphene.** Evolution of C1s XPS core level

203 spectra for growth of epitaxial graphene using FTF technique (a, c) as a function of growth temperature and

204 (b,d) growth time on on-axis and off-axis SiC respectively. S1 and S2 are the contributions of the buffer layer.

205 **3. Time evolution of the growth**

206 The evolution of Graphene and SiC components of XPS C1s core level spectra was

207 investigated as a function of time at different annealing temperatures to understand the

208 growth mechanism of epitaxial graphene. Figure 3a and 3b show the sample evolution of the

209 C1s peak as a function of time for epitaxial graphene grown at 1350 ˚C and 1400 ˚C on on-

210 axis and off-axis SiC respectively. The relative intensity of graphene and SiC components

211 change by time and as the growth time increases, the intensity of graphene peak increases due

212 to the development of the graphene

213 layers.

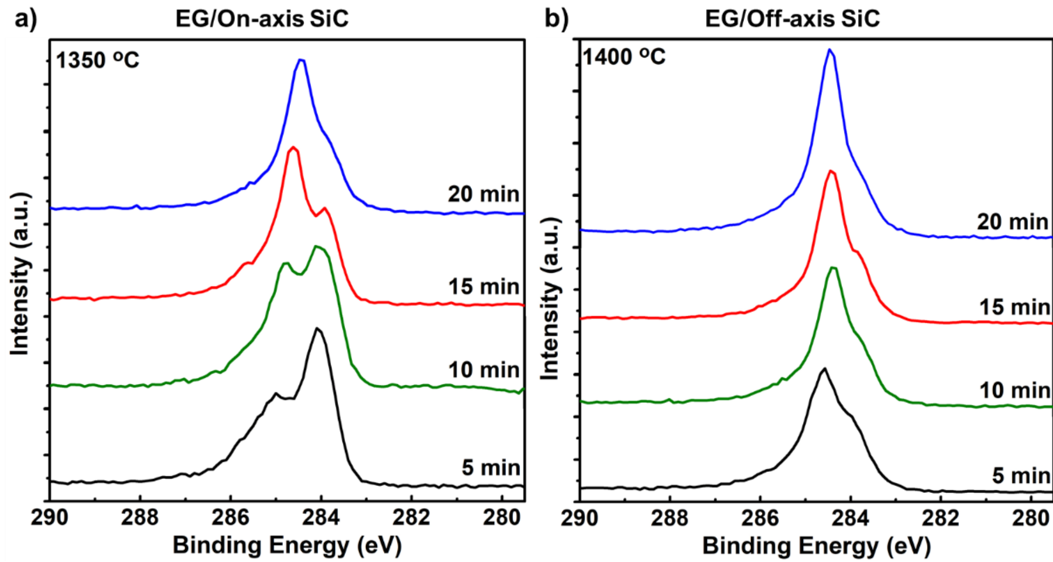

214 **Figure 3. XPS time evolution of FTF grown epitaxial graphene.** Time evolution of XPS C1s core level
215 spectra for epitaxial graphene grown on (a) on-axis SiC and (b) off-axis SiC at 1350 ˚C and 1400 ˚C
216 respectively.

217 Here we analyse the growth of epitaxial graphene considering the Frank Van der Merwe model
218 which applies to the layer-by layer growth of thin films. This model considers the evolution of
219 epitaxial graphene when the Si atoms leave the surface and the C atoms form 2D graphene
220 islands [51]. Defects, polishing sites and step edges of SiC are potential nucleation sites: the
221 first 2D graphene islands start to form around these nucleation sites and increase their size to
222 build the first graphene layer. Si atoms keep escaping step edges and the defects on the surface
223 leading to the formation of other graphene layers on top of the buffer layer which is an interface
224 layer partially connected to the Si atoms of SiC [52]. Considering the Frank Van der Merwe
225 growth model, the kinetics are described by the equation:

226 $$\frac{dn}{dt} = K(T)f(n), \qquad (2)$$

227 where n is the number of layers, $K(T)$ is the rate constant of the process, and $f(n)$ is a function
228 of the number of layers. The function $f(n)$ depends on the mechanism of the reaction which
229 in this case involves diffusion of Si and C atoms across the solid phase for the formation of

230 graphene. As the speed of the reaction decreases with the increase of the number of layers, we

231 have

232 $$f(n) = \frac{b}{n},\qquad (3)$$

233 where b is a constant. This function accounts for the increasing difficulty of Si atoms in leaving

234 the surface as the number of graphene layers increases. The kinetics of reaction $K(T)$ can be

235 expressed as:

236 $$K(T) = v\, e^{-Ea/kT}\qquad (4)$$

237 Where v is a pre-exponential factor, E_a is the activation energy and k is the Boltzmann constant

238 (8.617×10^{-5} eV K^{-1}). From equation 2 and 3 the following well-known parabolic kinetics can

239 be obtained:

240 $$n\, dn = K(T) b\, dt\qquad (5)$$

241 The integral of equation 5 is $n^2 + const = K(T)b\, t + const$ and by assuming the constants

242 as zero (n=0 for t=0) we obtain:

243 $$n \propto K(T)^{1/2}\, t^{1/2} = v^{1/2}\, e^{-Ea/2kT} t^{1/2}\qquad (6)$$

244 The number of graphene layers developed on on-axis and off-axis SiC by annealing at different

245 temperatures is plotted as a function of growth time as shown in Figure 4a and 4b respectively.

246 The data in Figure 4a and 4b are fitted using the following power growth law and the value of

247 β for each temperature is determined as [53].

248 $$n(t) = \beta\sqrt{t}\qquad (7)$$

249 By using the β values as parameters of equation 6 and plotting the Arrhenius plots: *ln(β)* vs

250 $1/2\ (kT)$ (Figure 4c and 4d), the activation energies of 4.06 ± 0.57 eV and 3.62 ± 1.32 eV

251 are obtained for growth on on-axis and off-axis SiC respectively. The obtained β values at

252 different temperatures are given in Table 2. The activation energy values obtained in this study
253 are similar to the values reported in our previous paper for the growth of epitaxial graphene on
254 3C SiC/Si(111) [54]. Concerning the activation energy extracted from the kinetics of Figure 4,
255 it is expected to be made up of several contributions. As described earlier, the formation of the
256 graphene layers is a multi- step process involving the sublimation of Si, via diffusion through
257 the forming layer, with generation of C atoms for the growth of the graphene phase. We
258 proposed a kinetic approach for the graphene growth in vacuum at high temperature, by
259 modeling Si diffusion in the layer via defects formation [54]. Specifically, the following
260 reactions were considered for sublimation and growth

261 $$SiC \rightarrow (Si)_v + C^* \qquad (8)$$

262 $$C^* + G_n \rightarrow G_{n+1} \qquad (9)$$

263 where $(Si)_v$ is a Si atom in the gas phase, C* a "reactive" C atom and G_n a graphene layer
264 made up of n-Carbon units. The solution of the kinetics provides the time dependence of the
265 thickness of the overlayer. Moreover, it was shown that the parabolic law (Equation 7) is
266 attained for $\exp[-(U_d^* + \frac{E_{Si}}{2} - U_{C^*})/kT] \cong \exp[-(U_d^* + \frac{E_{Si}}{2})/kT]$, where U_d^* is the activation
267 energy for Si diffusion, E_{Si} the energy for Si vacancy formation at the interface and U_{C^*} the
268 activation energy for the kinetic step (Equation 9). Accordingly, it follows that Ea, in Equation
269 6, can be identified with $U_d^* + \frac{E_{Si}}{2}$. The slight decrease of this quantity, on going from on-axis
270 to off-axis sample, can be ascribed to the larger step density which may reduce the energy for
271 defect formation.

272

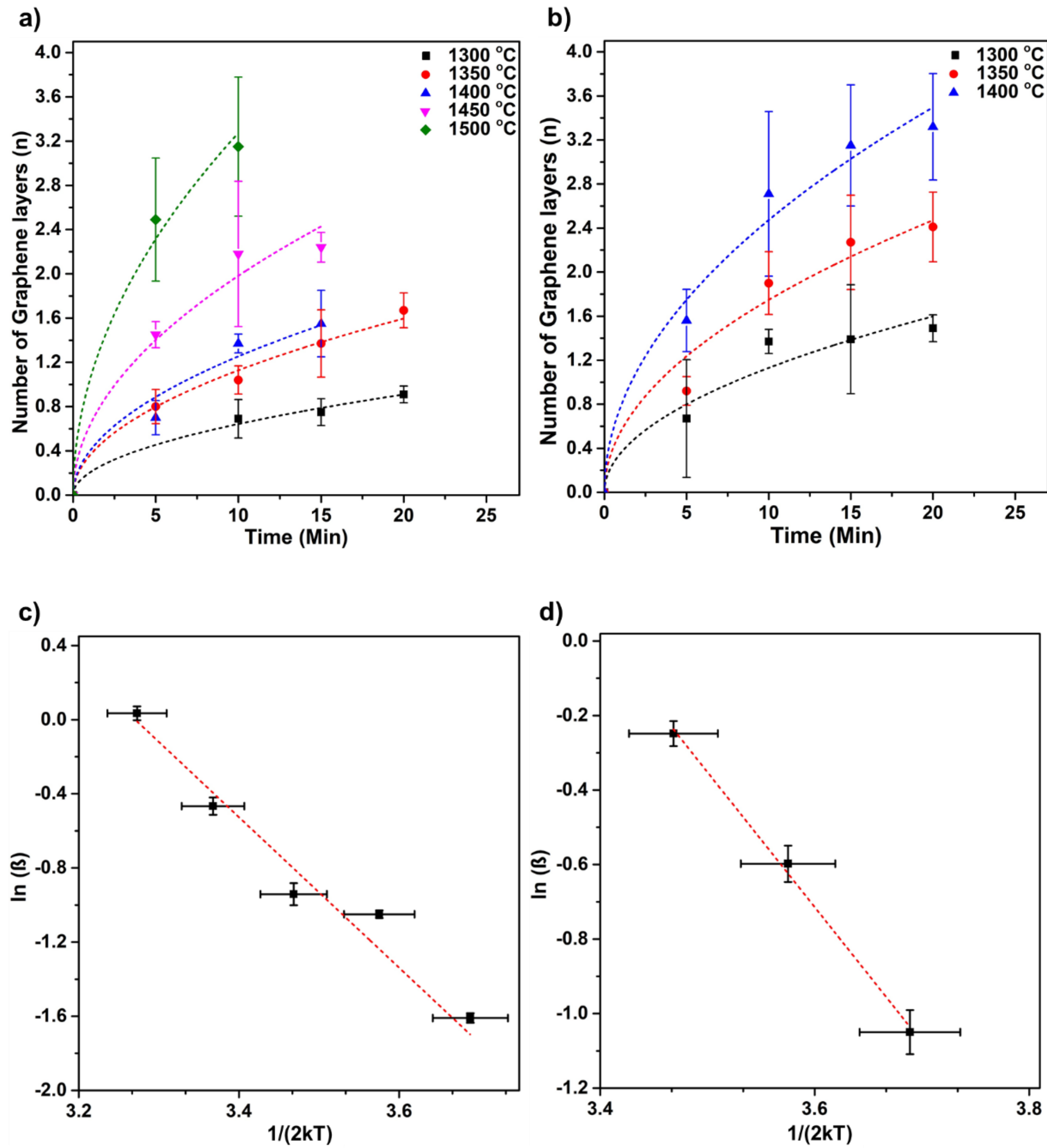

273 **Figure 4. Evolution of the growth rate for FTF grown epitaxial graphene.** Time dependence of developed
274 graphene layers on (a) on-axis SiC and (b) off-axis SiC at different annealing temperatures. (c) and (d)
275 correspond to the Arrhenius plots of the fitting parameter β (ln(β) vs 1/2kT) obtained from (a) and (b)
276 respectively.

277

278 **Table 2. Calculated parameter from the evolution of growth rate analysis.** Values of β obtained from the
279 fitting of n (t) using equation 6 at different temperatures for the growth of epitaxial graphene on on-axis and off-
280 axis SiC by FTF technique.

	T(˚C)	β ($min^{-1/2}$)	σ ($\times 10^{-2}$)

On-axis	SiC	1300	0.203	0.51
		1350	0.357	0.82
		1400	0.396	2.32
		1450	0.627	2.91
		1500	1.035	3.91
Off-axis	SiC	1300	0.357	2.07
		1350	0.552	2.67
		1400	0.782	2.62

281

282 **4. Atomic force microscopy**

283 The morphology of the epitaxial graphene grown on on-axis and off-axis SiC at different
284 annealing temperatures and growth times has been studied by atomic force microscopy in
285 tapping mode. Figure S3 and S4 include the full set of AFM images acquired on on-axis and
286 off-axis SiC after annealing at all the different growth temperatures and times. For epitaxial
287 graphene on on-axis SiC, the samples with the widest terrace size are obtained at 1280 ˚C, 1300
288 ˚C, and 1350 ˚C for 20, 15 and 10 minutes respectively, as shown in Figure 5 (a-c). The sample
289 shown in Figure 5b shows the surface with the most uniform wide terraces (up to 5µm width)
290 covered by 0.75 graphene layers. This sample is representative of the growth in optimum
291 conditions (1300 ˚C and 15 minutes respectively). The growth at 1300 ˚C for 20 minutes creates
292 terraces up to 13 µm wide with 0.91 layers of graphene.

293 As the temperature increases, a shorter growth time is required to obtain one layer of epitaxial
294 graphene. However, the samples annealed at higher temperatures show less uniform terraces
295 with finger-like protrusions. Moreover, by increasing the annealing temperature, the density of
296 pits and nonuniformity of steps increases as a function of growth time. Many works have

297 reported these types of structures previously, which form due to rapid sublimation of Si [55-
298 59]. The formation of pits can be controlled by the mechanism of growth, and it has a very
299 strong influence on the nucleation of graphene. Here the growth of epitaxial graphene is well
300 controlled by the FTF technique with the best results obtained at 1300 ˚C for 20 minutes (Figure
301 5b). In these conditions the formation of pits is limited as the slow growth at 1300 ˚C allows
302 for the formation of large domains of buffer layer which have enough time to cover the SiC
303 steps before the first graphene layer develops. We argue that the Si counter pressure over the
304 surface provided by the FTF technique reduces the growth rate of epitaxial graphene and helps
305 the formation of uniform epitaxial graphene on SiC at optimum growth condition. As shown
306 in Figure S3, for growth at temperatures higher than 1300 ˚C, the density of pits decreases as
307 the annealing temperature increase for a certain growth time. Formation of pits initiates by
308 nonuniform growth of buffer layer of 6√3 structure on each SiC step of √3 structure and having
309 the SiC steps to continue to the next terrace. By increasing the annealing temperature, the
310 density of nucleation sites for formation of the buffer layer increases and closely tied small
311 domains cover the surface which greatly decreases formation of pits [60, 61]. Finger-like
312 structures appear on the steps of epitaxial graphene grown at 1400 ˚C for 10 minutes as shown
313 in Figure S3. Borovikov and Zangwill reported that the instability between the capillary
314 smoothing forces and the roughening forces driven from evaporation-condensation and
315 diffusion mechanism of atoms at the step edge results in formation of finger-like structures
316 [62]. For a certain pressure, they define a graphitization temperature (T_g) below which
317 graphene doesn't grow and a stability temperature (T_s) over which the growth is stable and the
318 structure of graphene steps is uniform. For temperatures between T_g and T_s ($T_g < T < T_s$) the
319 growth is unstable and the finger-like structures form. As the background pressure in the
320 chamber increases, the temperature window of unstable growth gets smaller up to a point where
321 the growth is fully stable at $T > T_g$ and $T_g = T_s$. This mechanism is connected to the stability

322 between the pressure originated by the sublimation of Si from the SiC surface and the
323 background pressure of the growth chamber which determines the average velocity of steps
324 movement in the kinetic theory. In the present work the epitaxial graphene growth is performed
325 under UHV, and finger-like structures are rarely observed across the temperatures and growth
326 times explored. Tapping mode AFM and KPFM images of a partially graphitised on-axis SiC
327 surface prepared by face-to-face annealing at 1300 °C for 5 minutes are shown in Figure S6 to
328 show different phases of the growth on the SiC surface. Figure S7 shows the plots of the line
329 profiles taken along an identical path from height, phase and contact potential difference (CPD)
330 channels , corresponding to the black, blue and red paths in Figure S6 (a)-(c). While variations
331 in the graphene layer thickness are unclear in the height channel (Figure S6(a)), the CPD in
332 Figure S6(c) clearly shows three contrast levels which correspond to the SiC substrate (low
333 CPD), monolayer graphene, and bilayer or multilayer graphene (high CPD). In summary it
334 seems that the FTF technique has helped to effectively stabilize the growth and to control the
335 structure of graphene steps.

336 Figure 6 (a-c) shows the AFM images of epitaxial graphene grown on off-axis SiC at 1300 ˚C,
337 1350 ˚C and 1400 ˚C for 15, 10 and 5 minutes respectively. In this case, annealing at 1350 ˚C
338 for 10 minutes is the optimised growth condition, resulting in 1.9 layers of graphene and terrace
339 width of up to 440 nm which is the sample with the widest continuous steps and minimum
340 number of graphene layers at the same time. All the AFM images of the samples grown on off-
341 axis SiC at various growth temperatures and time show pit-free structures (Figure S4).
342 However, monolayer or bilayer graphene islands can be seen on the steps of epitaxial graphene
343 grown at 1350 ˚C for 20 minutes (Figure S5). We believe that these structures are formed when
344 the steps of SiC retract due to decomposition. As the SiC retracts and joins the adjacent SiC
345 step, it leaves behind the earlier formed graphene layers as islands while some of the graphene
346 islands continue to grow. This process continues while the SiC terraces continue to retract to

347 join other SiC steps and the nucleated graphene islands grow to form continuous graphene
348 layers [63]. The surface morphology of epitaxial graphene grown by standard technique on on-
349 axis and off-axis SiC by annealing at 1300 ˚C for 1 minute are shown in the Figure S2 STM
350 images that are obtain in-situ after growth in UHV system. In this technique, epitaxial graphene
351 on on-axis SiC (Figure S2a) shows a nonuniform and discontinuous island with defects such
352 as pits and wrinkles. On the other hand, epitaxial graphene on off-axis SiC shows continuous
353 but very narrow (up to 10 nm) terraces covered by wrinkles. Comparing the morphology of
354 FTF grown epitaxial graphene with the samples grown by standard technique, it is proven that
355 the structure of epitaxial graphene grown both on on-axis and off-axis SiC is significantly
356 improved by FTF method in terms of uniformity, quality, and size of terraces.

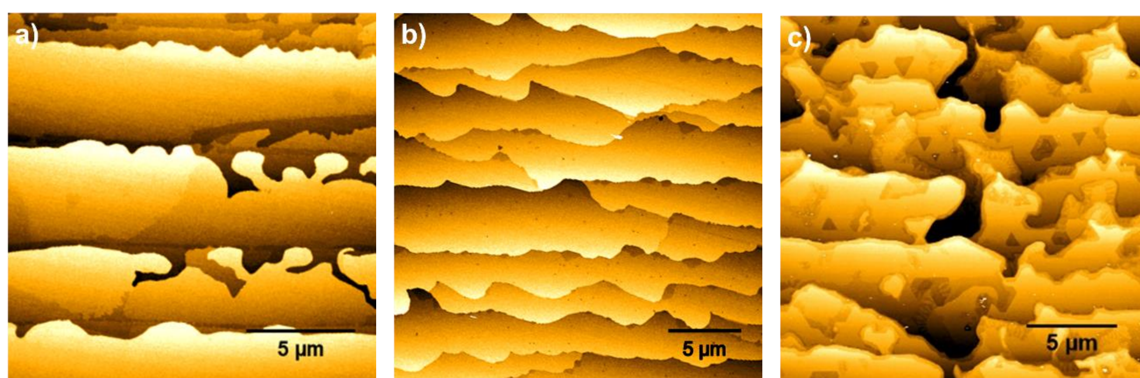

357 **Figure 5. Morphology analysis of FTF grown epitaxial graphene on on-axis SiC.** AFM topography of
358 Epitaxial graphene on on-axis SiC grown at (a)1280 ˚C for 20 mins, (b) 1300 ˚C for 15 mins, and (c) 1350 ˚C
359 for 10 minutes.

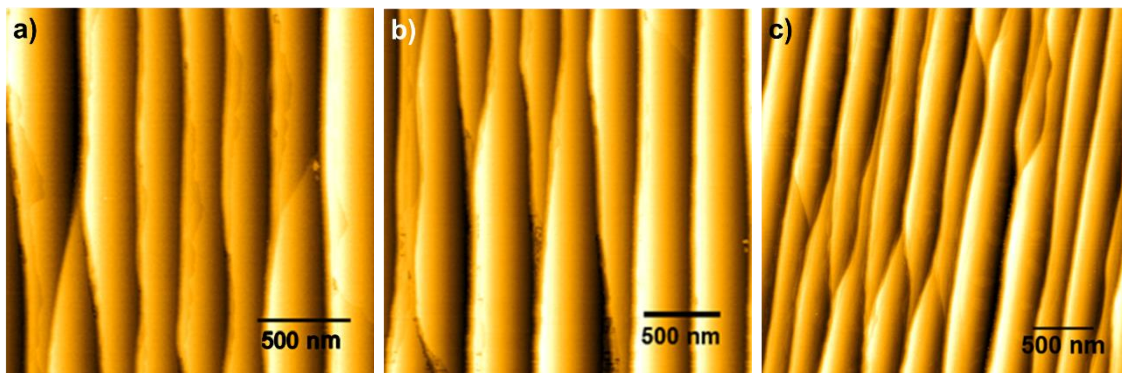

360 **Figure 6. Morphology analysis of FTF grown epitaxial graphene on off-axis SiC.** AFM topography of
361 Epitaxial graphene on off-axis SiC grown at (a)1300 ˚C for 15 mins, (b) 1350 ˚C for 10 mins, and (c) 1400 ˚C
362 for 5 minutes.

363 ## 5. Scanning tunnelling microscopy

364 Atomically resolved STM images of epitaxial graphene grown on on-axis SiC at 1300 ˚C for
365 15 minutes and on off-axis SiC at 1350 ˚C for 10 minutes (optimised growth conditions) are
366 shown in Figure 7a and 7b respectively. The (1×1) graphene lattice structure is clearly visible
367 and marked in green in the zoomed-in images (insets) in Figure 7a and 7b. The line profile
368 along the red line indicated on both Figures 7a and 7b is represented below each graph and
369 shows the atomic periodicity of 0.241±0.005 nm and 0.239±0.005 nm respectively which
370 closely matches the graphene lattice parameter (0.246 nm). Figure 7a shows the superposition
371 of (6√3×6√3)R30˚ moiré pattern (blue unit cell) and graphene honeycomb lattice structure of
372 monolayer graphene. The moiré superlattice, which arises due to the rotation of the
373 (6√3×6√3)R30˚ reconstructed buffer layer with respect to the SiC(0001) substrate, has a
374 periodicity of about 18 Å [64, 65], which is not very clear in Figure 7b as the number of
375 graphene layers is higher with respect to 7a and only a shadow of the Moiré pattern is visible.
376 The FFTs of Figures 7a and 7b are shown in Figures 7c and 7d respectively. Both Figures 7c
377 and 7d show the pattern containing three sets of bright spots which corresponds to
378 (6√3×6√3)R30˚ (buffer layer) , graphene and the Moiré pattern. The angle between the first
379 and the second set of spots shows the orientation of epitaxial graphene with respect to

380 $(6\sqrt{3}\times6\sqrt{3})R30^{\circ}$. In Figure 7c this rotation is 29.0° ± 0.5° with respect to the SiC substrate (on-
381 axis SiC). For off-axis SiC, the rotation of graphene is 32.0° ± 0.2° (Figure 7d). An analysis of
382 the various components of the FFT transform (Figure 7c and 7d) is shown in Figure S8. The
383 back Fourier Transform of the central, middle and outermost hexagons as marked in the FFT
384 inset images of Figure S8 provide the real space image of the moiré pattern, second nearest
385 neighbour and first nearest neighbour atoms respectively.

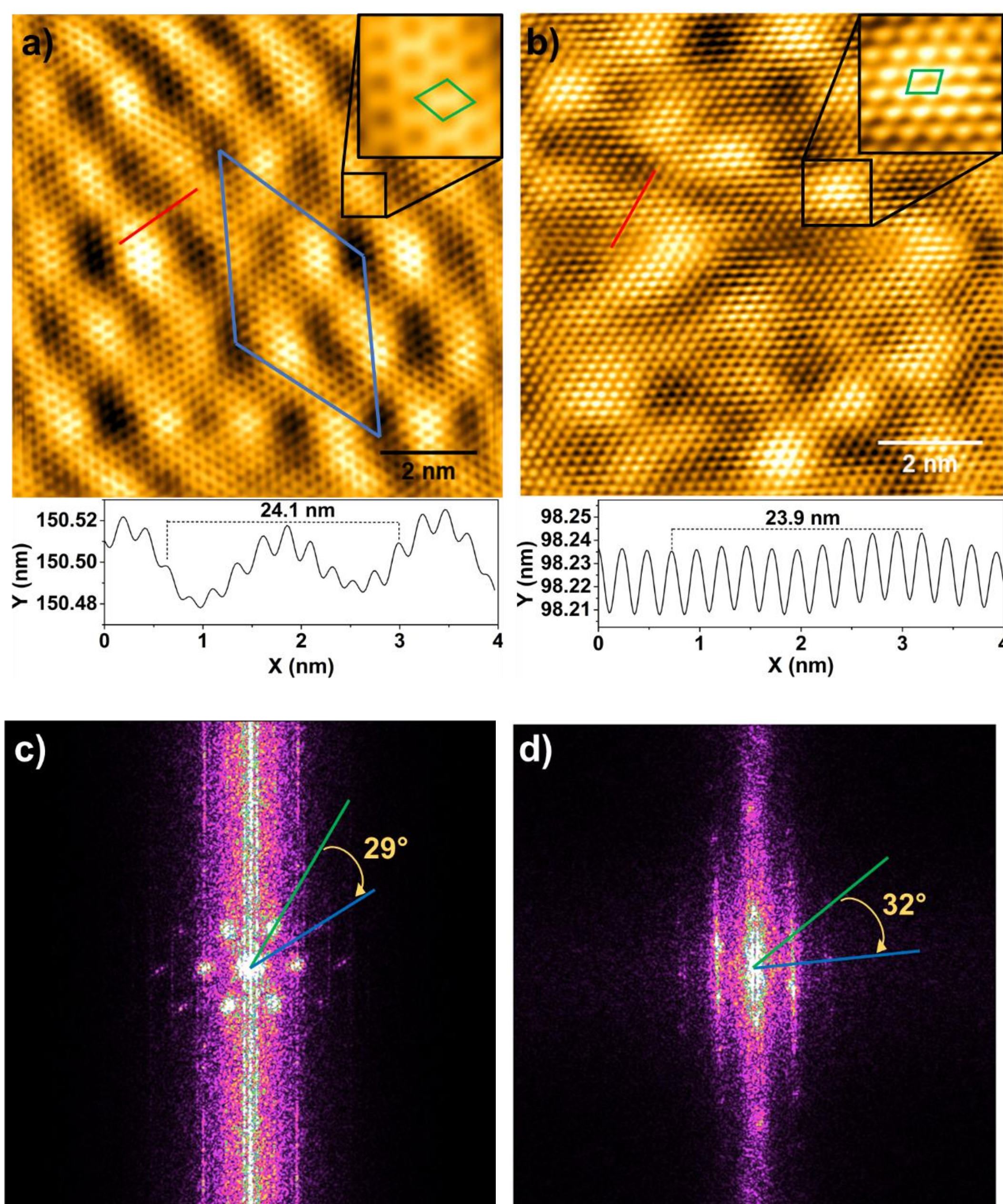

386 **Figure 7. STM characterization of FTF grown epitaxial graphene.** (10×10) nm^2 atomic resolution STM
387 images of epitaxial graphene grown by FTF technique on (a) on-axis SiC (U= -0.9 V; I= 0.03 nA) and (b) off-

388 axis SiC (U= - 0.6 V; I= 0.7 nA) at optimised growth conditions of annealing at 1300 ˚C for 15 mins and 1350
389 ˚C for 10 minutes respectively. (a) shows Moiré pattern with hexagonal symmetry and $(6\sqrt{3}\times6\sqrt{3})R30°$ unit cell
390 which is marked in blue. The insets show the zoom-in of the STM images with graphene unit cells marked as
391 green. The atomic corrugation of graphene is represented by the line profiles along the red lines (c) and (d)
392 shows the respective FFT images of (a) and (b).

393

394 ## 6. Raman spectroscopy

395 Raman analysis of the FTF grown epitaxial graphene on both on-axis and off-axis SiC has been
396 performed ex-situ after the growth. The Raman spectra are shown in Figure 8 and Figure 9
397 respectively. Figure 8a shows the evolution of the Raman spectrum as a function of temperature
398 for epitaxial graphene grown on on-axis SiC for 15 min. Three characteristic Raman peaks of
399 D, G and 2D are labelled on the spectra. The Raman peaks of epitaxial graphene and SiC
400 overlap and as the intensity of the G and D peaks of epitaxial graphene are very small in
401 comparison with the SiC peaks, it is very difficult to discern them. The 2D peak however, is
402 located at a higher wavenumber, where there are no SiC reference peaks and the changes in
403 this peak can be easily tracked. For epitaxial graphene on SiC we cannot define the number of
404 graphene layers simply by looking at the shape of the 2D and G characteristic peaks in the raw
405 Raman spectra [66]. To make the G and D peaks in Figure 8a more distinct, the Raman spectra
406 of untreated on-axis 4H-SiC is partially subtracted from the Raman spectra of all samples as
407 shown in Figure 8b as suggested by Röhrl et al [67]. The D, G and 2D peaks do not appear on
408 the Raman spectra for epitaxial graphene grown on on-axis SiC at 1280 ˚C and 1300 ˚C for 15
409 min as the number of graphene layers is less than one (0.31 and 0.75 respectively). The intensity
410 of D peak in Figure 8a and Figure 8b Raman spectra is very small for all samples which
411 confirms the excellent crystalline quality of our epitaxial graphene grown on on-axis SiC by
412 FTF technique. Figure 8b shows that as the number of graphene layers are increased by
413 increasing the annealing temperature from 1350 ˚C to 1450 ˚C, the wavenumber for D peak

414 increases from 1353 cm^{-1} (1.37 layers) to 1378 cm^{-1} (2.24 layers). The position of G peak
415 doesn't change by temperature and is located around 1606 cm^{-1}. As shown in Figure 8b, the
416 intensity of G peak increases by annealing temperature and indicates increase in the number of
417 graphene layers. The position of 2D peak shifts from 2720 to 2745 cm^{-1} with increase in
418 annealing temperature and consequently the number of graphene layers from 1350 ˚C to 1450
419 ˚C (Figure 8a). Figure 8c shows the Raman spectra as a function of growth time for growth of
420 epitaxial graphene on on-axis SiC at 1300 ˚C. By comparing the Raman spectra of plain on-
421 axis SiC with the epitaxial graphene grown at 1300 ˚C for 10 minutes, we can see that the D,
422 G and 2D peaks are absent as the number of layers is 0.69. As the growth time increases from
423 10 to 15 minutes (0.75 layers), no 2D peaks appear but a very low intensity G peak can be seen
424 in the background subtracted Raman spectra (Figure 9d). For 20 minutes of growth the 2D peak
425 appears at 2718 cm^{-1} (Figure 8c) and the G and the very small intensity D peaks are seen at
426 1605 and 1349 cm^{-1} respectively (Figure 8d). The same increasing trend for 2D peak as growth
427 on on-axis SiC can be seen for growth on off-axis SiC in Figure 9a and the position of this peak
428 increases with the growth temperature. For growth at 1300 ˚C, 1350 ˚C and 1400 ˚C the position
429 of 2D peak is 2725, 2729 and 2743 cm^{-1} respectively. The D and G peaks are shown in Figure
430 9b after subtraction SiC background for each annealing temperature. The position of G is at ~
431 1606 cm^{-1} for all the samples. The small intensity D peaks for all samples again indicates the
432 high quality of epitaxial graphene grown on off-axis SiC. The position of D peak also increases
433 by the number of graphene layers and by increasing the annealing temperature or the growth
434 time (Figure 9b, 9d). The Raman spectra around the D and G peaks for epitaxial graphene
435 grown by FTF technique on on-axis and off-axis SiC at optimised growth conditions of
436 annealing at 1300 ˚C for 15 mins and 1350 ˚C for 10 minutes as well as epitaxial graphene
437 grown by standard technique on on-axis and off-axis SiC by annealing at 1300 ˚C for 1 minute
438 are shown in Figure S9. The intensity of D peak for FTF grown epitaxial graphene on both on-

439 axis and off-axis SiC is negligible in comparison to the epitaxial graphene grown by standard
440 technique on on-axis and off-axis SiC. This confirms high quality of epitaxial graphene grown
441 by FTF technique and how the presence of defects are notably diminished in this method. The
442 FTF technique is a simple way to overcome two common causes of defect formation in growth
443 of epitaxial graphene on SiC in UHV that are low growth temperature and fast Si evaporation
444 from the SiC surface [42]. Control over the growth rate and fast sublimation of Si in UHV is
445 achieved by the counter pressure toward the surface of SiC in FTF growth technique which
446 provides equilibrium in the sublimation process by reducing the Si evaporation rate which
447 consequently prevents the formation of defects on the surface by slow reconfiguration of C
448 atoms for formation of high quality graphene crystal [68].

449

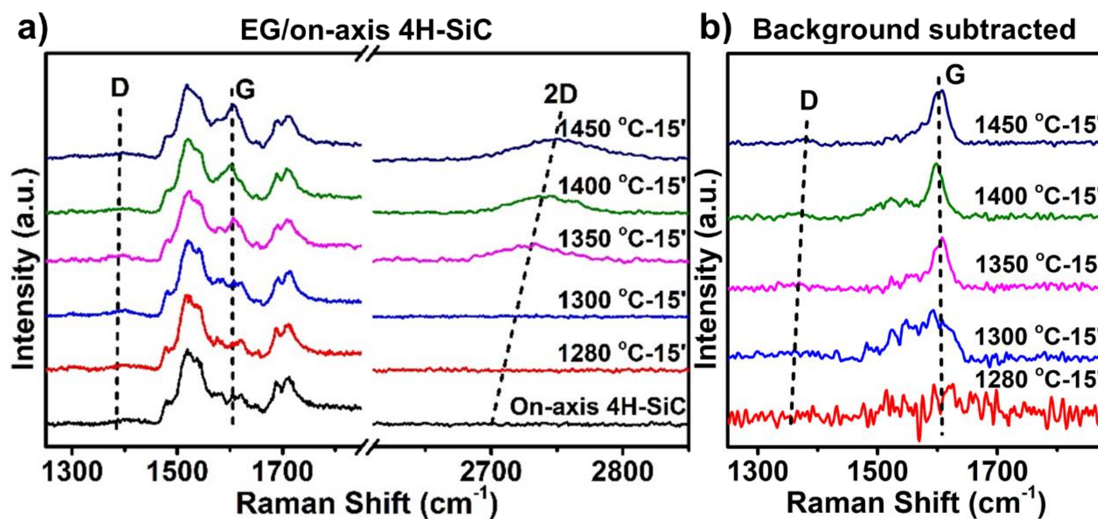

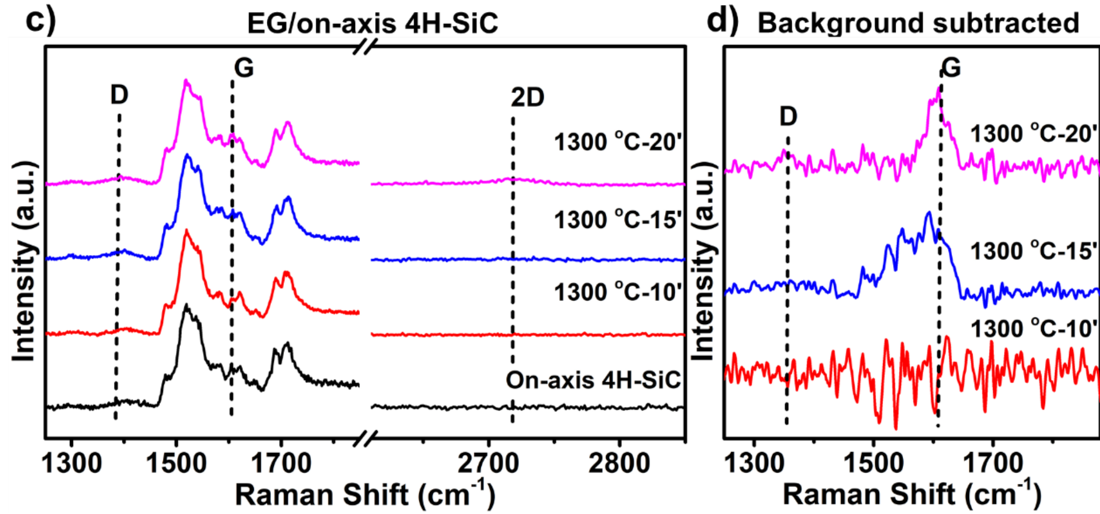

450 **Figure 8. Raman characterization of FTF grown epitaxial graphene on on-axis SiC.** The evolution of
451 Raman spectra as a function of (a) annealing temperature and (c) growth time for FTF growth of epitaxial
452 graphene on on-axis SiC with the on-axis 4H-SiC(0001) reference. (b) and (d) The Raman spectra around the D
453 and G peaks for the samples shown in (a) and (c) respectively with the partial subtraction of bare SiC Raman
454 spectra as background.

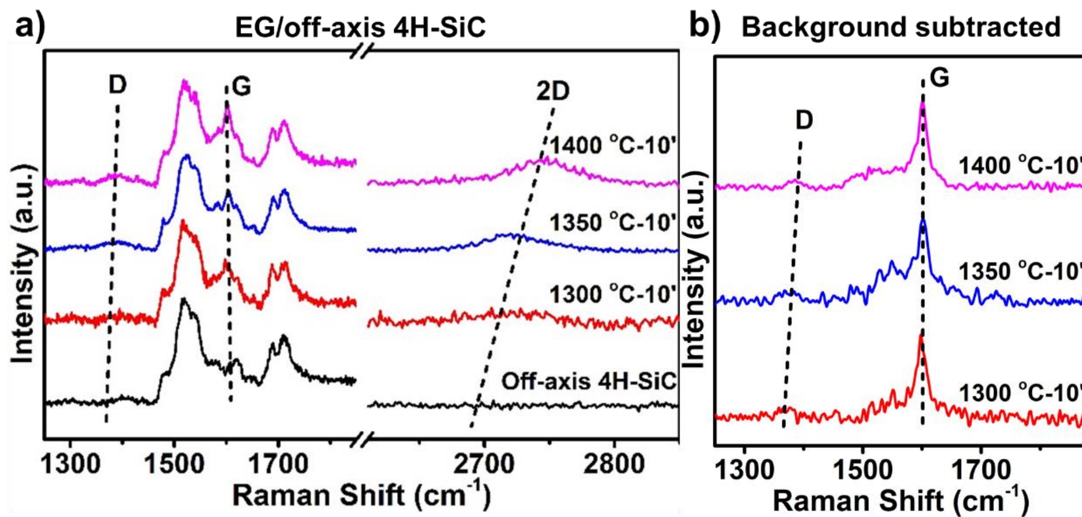

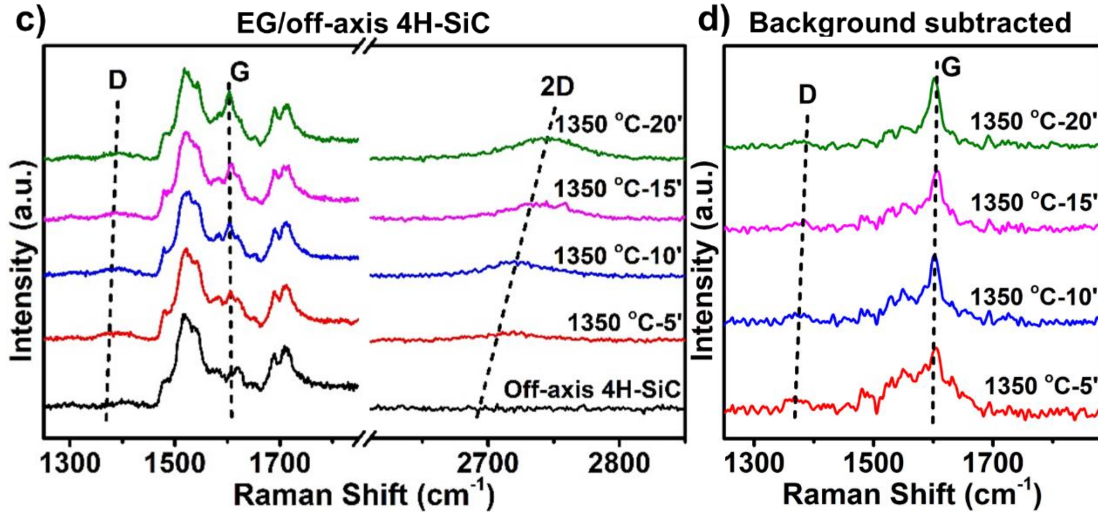

455 **Figure 9. Raman characterization of FTF grown epitaxial graphene on off-axis SiC.** The evolution of
456 Raman spectra as a function of (a) annealing temperature and (c) growth time for FTF growth of epitaxial
457 graphene on off-axis SiC with the off-axis 4H-SiC(0001) reference. (b) and (d) The Raman spectra around the D
458 and G peaks for the samples shown in (a) and (c) respectively with the partial subtraction of bare SiC Raman
459 spectra as background.

460 ## 7. Conclusion

461 A novel face-to-face (FTF) growth technique is explored to control the growth of epitaxial
462 graphene in UHV condition. The growth on both on-axis and off-axis SiC is optimised and the
463 best annealing temperature and growth time are reported. Epitaxial graphene grown on on-axis
464 SiC at 1300 ˚C for 15 minutes shows the most uniform and widest terraces (up to 5μm). The
465 growth on off-axis SiC at 1350 ˚C for 10 minutes show the widest terraces (up to 440 nm). The
466 FTF techniques proves to be very effective in controlling the growth rate and structure of
467 epitaxial graphene under UHV by decreasing the rate of Si sublimation from the surface via
468 the counter pressure generated by Si sublimation in the space between the two SiC substrates.
469 The number of graphene layers is calculated for each annealing temperature using quantitative
470 XPS analysis and a growth model has been used to describe the evolution of the number of
471 layers as a function of time. The square root growth law obtained by fitting our data is an
472 indication of the layer-by-layer growth of epitaxial graphene. According to this law the kinetic

473 model shows that the rate declines as a function of time because the development of graphene
474 layers hampers fast sublimation of Si, by limiting the pathways for the sublimation of Si which
475 occurs normally via defects and step edges. The activation energies are calculated based on the
476 kinetic model as 4.06 ± 0.57 eV and 3.62 ± 1.32 eV for the growth on on-axis and off-axis SiC
477 respectively. High resolution STM images show the high quality of graphene and the
478 superposition $(6\sqrt{3}\times6\sqrt{3})R30^{\circ}$ moiré pattern. The evolution of D and 2D peaks in Raman
479 spectroscopy are studied as a function of temperature and time. The very low intensity of D
480 peaks in the Raman spectra of all samples confirm the high quality of graphene grown by the
481 FTF technique.

482 The growth by the FTF technique provides an effective solution to obtain high-quality epitaxial
483 graphene on SiC in UHV, paving the way to its applications in 2D electronics.

484

485 **Acknowledgements**

486 N.Z. acknowledges the support form Australian Government Research Training Program
487 (RTP). Facilities at Central Analytical Research Facility (CARF) and the Faculty of Science
488 and the Faculty of Engineering that provide funding for all the research facilities in CARF are
489 kindly acknowledged. The authors acknowledge the facilities and support provided by
490 Australian National Fabrication Facility (ANFF) at University of Queensland (UQ). This work
491 has been partially supported by ARC through the Discovery Project DP200102546.

492

493

494

495

496 **References**

497 1. Das, P., S. Ganguly, S. Banerjee, and N.C. Das, *Graphene based emergent*
498 *nanolights: a short review on the synthesis, properties and application.* J Research on
499 Chemical Intermediates, 2019. **45**(7): p. 3823-3853.
500 2. Novoselov, K.S., A.K. Geim, S.V. Morozov, D. Jiang, Y. Zhang, S.V. Dubonos, I.V.
501 Grigorieva, and A.A. Firsov, *Electric Field Effect in Atomically Thin Carbon Films.*
502 2004. **306**(5696): p. 666-669.
503 3. Novoselov, K.S., A.K. Geim, S.V. Morozov, D.-e. Jiang, Y. Zhang, S.V. Dubonos,
504 I.V. Grigorieva, and A.A. Firsov, *Electric field effect in atomically thin carbon films.*
505 J science, 2004. **306**(5696): p. 666-669.
506 4. Inagaki, M., *Applications of graphite intercalation compounds.* Journal of Materials
507 Research, 1989. **4**(6): p. 1560-1568.
508 5. Cellini, F., F. Lavini, T. Cao, W. de Heer, C. Berger, A. Bongiorno, and E. Riedo,
509 *Epitaxial two-layer graphene under pressure: Diamene stiffer than Diamond.* J
510 FlatChem, 2018. **10**: p. 8-13.
511 6. Sitek, J., J. Plocharski, I. Pasternak, A.P. Gertych, C. McAleese, B.R. Conran, M.
512 Zdrojek, and W. Strupinski, *Substrate-induced variances in morphological and*
513 *structural properties of MoS2 grown by chemical vapor deposition on epitaxial*
514 *graphene and SiO2.* J ACS Applied Materials Interfaces, 2020. **12**(40): p. 45101-
515 45110.
516 7. Yang, Y., H. Hou, G. Zou, W. Shi, H. Shuai, J. Li, and X. Ji, *Electrochemical*
517 *exfoliation of graphene-like two-dimensional nanomaterials.* J Nanoscale, 2019.
518 **11**(1): p. 16-33.
519 8. Chuang, C., Y. Yang, S. Pookpanratana, C.A. Hacker, C.-T. Liang, and R.E.
520 Elmquist, *Chemical-doping-driven crossover from graphene to "ordinary metal" in*
521 *epitaxial graphene grown on SiC.* J Nanoscale, 2017. **9**(32): p. 11537-11544.
522 9. Min, J.-H., K.-H. Li, Y.-H. Kim, J.-W. Min, C.H. Kang, K.-H. Kim, J.-S. Lee, K.J.
523 Lee, S.-M. Jeong, D.-S. Lee, and interfaces, *Toward Large-Scale Ga2O3 Membranes*
524 *via Quasi-Van Der Waals Epitaxy on Epitaxial Graphene Layers.* J ACS applied
525 materials, 2021. **13**(11): p. 13410-13418.
526 10. Zhang, F., X. Chen, Z. Zuo, X. Qin, X. Xu, and X. Zhao, *High performance metal-*
527 *graphene-metal photodetector employing epitaxial graphene on SiC (0001) surface.* J
528 Journal of Materials Science: Materials in Electronics, 2018. **29**(6): p. 5180-5185.
529 11. Aslanidou, S., A. García-García, E. Prats, P. Godignon, and G. Rius, *Large*
530 *anisotropic single crystal epitaxial graphene flakes isolated from SiC wafers.*
531 12. Briggs, N., Z.M. Gebeyehu, A. Vera, T. Zhao, K. Wang, A.D.L.F. Duran, B. Bersch,
532 T. Bowen, K.L. Knappenberger, and J.A. Robinson, *Epitaxial graphene/silicon*
533 *carbide intercalation: a minireview on graphene modulation and unique 2D*
534 *materials.* J Nanoscale, 2019. **11**(33): p. 15440-15447.
535 13. Berger, C., Z. Song, T. Li, X. Li, A.Y. Ogbazghi, R. Feng, Z. Dai, A.N. Marchenkov,
536 E.H. Conrad, P.N. First, and W.A. de Heer, *Ultrathin Epitaxial Graphite: 2D*
537 *Electron Gas Properties and a Route toward Graphene-based Nanoelectronics.* The
538 Journal of Physical Chemistry B, 2004. **108**(52): p. 19912-19916.
539 14. Somani, P.R., S.P. Somani, and M. Umeno, *Planer nano-graphenes from camphor by*
540 *CVD.* Chemical Physics Letters, 2006. **430**(1): p. 56-59.
541 15. Yi, K., D. Liu, X. Chen, J. Yang, D. Wei, Y. Liu, and D. Wei, *Plasma-Enhanced*
542 *Chemical Vapor Deposition of Two-Dimensional Materials for Applications.*
543 Accounts of Chemical Research, 2021. **54**(4): p. 1011-1022.

16. Son, M., J. Jang, G.-H. Kim, J.-H. Lee, D.W. Chun, J.-H. Bae, I.S. Kim, M.-H. Ham, and S.-S. Chee, *Large-Area Bernal-Stacked Bilayer Graphene Film on a Uniformly Rough Cu Surface via Chemical Vapor Deposition.* ACS Applied Electronic Materials, 2021. **3**(6): p. 2497-2503.
17. Emtsev, K.V., A. Bostwick, K. Horn, J. Jobst, G.L. Kellogg, L. Ley, J.L. McChesney, T. Ohta, S.A. Reshanov, J. Röhrl, E. Rotenberg, A.K. Schmid, D. Waldmann, H.B. Weber, and T. Seyller, *Towards wafer-size graphene layers by atmospheric pressure graphitization of silicon carbide.* Nature Materials, 2009. **8**(3): p. 203-207.
18. Ciochoń, P., M. Marzec, N. Olszowska, and J. Kołodziej, *Reversible graphitization of SiC: A route towards high-quality graphene on a minimally step bunched substrate.* J Applied Surface Science, 2020. **528**: p. 146917.
19. Ben-Gouider-Trabelsi, A., *Outstanding properties of epitaxial graphene grown from silicon carbide substrate*. Loughborough University.
20. Badami, D.V., *Graphitization of α-Silicon Carbide.* Nature, 1962. **193**(4815): p. 569-570.
21. Kim, M., M. Hupalo, M.C. Tringides, B. Schrunk, A. Kaminski, K.-M. Ho, and C.-Z. Wang, *Electronic structure of double-layer epitaxial graphene on SiC (0001) modified by Gd intercalation.* J The Journal of Physical Chemistry C, 2020. **124**(51): p. 28132-28138.
22. Kruskopf, M., D.M. Pakdehi, K. Pierz, S. Wundrack, R. Stosch, T. Dziomba, M. Götz, J. Baringhaus, J. Aprojanz, C. Tegenkamp, J. Lidzba, T. Seyller, F. Hohls, F.J. Ahlers, and H.W. Schumacher, *Comeback of epitaxial graphene for electronics: large-area growth of bilayer-free graphene on SiC.* 2D Materials, 2016. **3**(4): p. 041002.
23. Zhou, S.Y., G.-H. Gweon, A. Fedorov, P. First, de, W. De Heer, D.-H. Lee, F. Guinea, A. Castro Neto, and A. Lanzara, *Substrate-induced bandgap opening in epitaxial graphene.* J Nature materials, 2007. **6**(10): p. 770-775.
24. De Heer, W.A., C. Berger, X. Wu, M. Sprinkle, Y. Hu, M. Ruan, J.A. Stroscio, P.N. First, R. Haddon, and B. Piot, *Epitaxial graphene electronic structure and transport.* J Journal of Physics D: Applied Physics, 2010. **43**(37): p. 374007.
25. Virojanadara, C., R. Yakimova, J. Osiecki, M. Syväjärvi, R. Uhrberg, L. Johansson, and A. Zakharov, *Substrate orientation: A way towards higher quality monolayer graphene growth on 6H-SiC (0 0 0 1).* J Surface Science, 2009. **603**(15): p. L87-L90.
26. Mikoushkin, V., V. Shnitov, A. Lebedev, S. Lebedev, S.Y. Nikonov, O.Y. Vilkov, T. Iakimov, and R. Yakimova, *Size confinement effect in graphene grown on 6H-SiC (0 0 0 1) substrate.* J Carbon, 2015. **86**: p. 139-145.
27. Daas, B., S.U. Omar, S. Shetu, K.M. Daniels, S. Ma, T. Sudarshan, M. Chandrashekhar, and design, *Comparison of epitaxial graphene growth on polar and nonpolar 6H-SiC faces: On the growth of multilayer films.* J Crystal growth, 2012. **12**(7): p. 3379-3387.
28. Yakimova, R., C. Virojanadara, D. Gogova, M. Syväjärvi, D. Siche, K. Larsson, and L.I. Johansson, *Analysis of the Formation Conditions for Large Area Epitaxial Graphene on SiC Substrates.* Materials Science Forum, 2010. **645-648**: p. 565-568.
29. Hass, J., J.E. Millán-Otoya, P.N. First, and E.H. Conrad, *Interface structure of epitaxial graphene grown on 4H-SiC(0001).* Physical Review B, 2008. **78**(20): p. 205424.
30. Hass, J., F. Varchon, J.E. Millán-Otoya, M. Sprinkle, N. Sharma, W.A. de Heer, C. Berger, P.N. First, L. Magaud, and E.H. Conrad, *Why Multilayer Graphene on $4H\mathrm{\text{\ensuremath{-}}}\mathrm{SiC}(000\overline{1})$ Behaves Like a Single Sheet of Graphene.* Physical Review Letters, 2008. **100**(12): p. 125504.

594 31. Tedesco, J.L., B. VanMil, R.L. Myers-Ward, J. Culbertson, G. Jernigan, P. Campbell,
595 J.M. McCrate, S.A. Kitt, C. Eddy, and D.K. Gaskill, *Improvement of morphology and*
596 *free carrier mobility through argon-assisted growth of epitaxial graphene on silicon*
597 *carbide.* J ECS Transactions, 2009. **19**(5): p. 137.
598 32. Jin, L., Q. Fu, H. Zhang, R. Mu, Y. Zhang, D. Tan, and X. Bao, *Tailoring the growth*
599 *of graphene on Ru (0001) via engineering of the substrate surface.* J The Journal of
600 Physical Chemistry C, 2012. **116**(4): p. 2988-2993.
601 33. Drowart, J., G.D. Maria, and M.G. Inghram, *Thermodynamic Study of SiC Utilizing a*
602 *Mass Spectrometer.* 1958. **29**(5): p. 1015-1021.
603 34. Hupalo, M., E. Conrad, and M. Tringides, *Growth mechanism for epitaxial graphene*
604 *on vicinal 6 H-SiC (0001) surfaces: A scanning tunneling microscopy study.* J
605 Physical review B, 2009. **80**(4): p. 041401.
606 35. Mishra, N., J. Boeckl, N. Motta, and F. Iacopi, *Graphene growth on silicon carbide:*
607 *A review.* J physica status solidi, 2016. **213**(9): p. 2277-2289.
608 36. Ahmed, M., M. Khawaja, M. Notarianni, B. Wang, D. Goding, B. Gupta, J.J. Boeckl,
609 A. Takshi, N. Motta, and S.E. Saddow, *A thin film approach for SiC-derived*
610 *graphene as an on-chip electrode for supercapacitors.* Nanotechnology, 2015. **26**(43):
611 p. 434005.
612 37. Gupta, B., E. Placidi, C. Hogan, N. Mishra, F. Iacopi, and N. Motta, *The transition*
613 *from 3C SiC(111) to graphene captured by Ultra High Vacuum Scanning Tunneling*
614 *Microscopy.* Carbon, 2015. **91**(0): p. 378-385.
615 38. Syväjärvi, M., R. Yakimova, and E. Janzén, *Step-bunching in 6H-SiC growth by*
616 *sublimation epitaxy.* J Journal of Physics: Condensed Matter, 1999. **11**(49): p. 10019.
617 39. Syväjärvi, M., R. Yakimova, and E. Janzén, *Interfacial properties in liquid phase*
618 *growth of SiC.* J Journal of the Electrochemical Society, 1999. **146**(4): p. 1565.
619 40. Hass, J., R. Feng, T. Li, X. Li, Z. Zong, W.A.d. Heer, P.N. First, E.H. Conrad, C.A.
620 Jeffrey, and C. Berger, *Highly ordered graphene for two dimensional electronics.*
621 2006. **89**(14): p. 143106.
622 41. Hass, J., W. De Heer, and E. Conrad, *The growth and morphology of epitaxial*
623 *multilayer graphene.* J Journal of Physics: Condensed Matter, 2008. **20**(32): p.
624 323202.
625 42. De Heer, W.A., C. Berger, M. Ruan, M. Sprinkle, X. Li, Y. Hu, B. Zhang, J.
626 Hankinson, and E. Conrad, *Large area and structured epitaxial graphene produced*
627 *by confinement controlled sublimation of silicon carbide.* J Proceedings of the
628 National Academy of Sciences, 2011. **108**(41): p. 16900-16905.
629 43. Ciochoń, P., Ł. Bodek, M. Garb, Ł. Zając, and J.J. Kołodziej, *Si beam-assisted*
630 *graphitization of SiC (0001).* Applied Physics A, 2018. **124**(10): p. 727.
631 44. Kim, M., J. Hwang, V.B. Shields, S. Tiwari, M.G. Spencer, and J.-W. Lee, *SiC*
632 *surface orientation and Si loss rate effects on epitaxial graphene.* Nanoscale research
633 letters, 2012. **7**(1): p. 186.
634 45. Yu, X., C. Hwang, C.M. Jozwiak, A. Köhl, A.K. Schmid, and A. Lanzara, *New*
635 *synthesis method for the growth of epitaxial graphene.* J Journal of Electron
636 Spectroscopy Related Phenomena, 2011. **184**(3-6): p. 100-106.
637 46. Fairley, N., V. Fernandez, M. Richard-Plouet, C. Guillot-Deudon, J. Walton, E.
638 Smith, D. Flahaut, M. Greiner, M. Biesinger, S. Tougaard, D. Morgan, and J.
639 Baltrusaitis, *Systematic and collaborative approach to problem solving using X-ray*
640 *photoelectron spectroscopy.* Applied Surface Science Advances, 2021. **5**: p. 100112.
641 47. Emtsev, K., F. Speck, T. Seyller, L. Ley, and J.D. Riley, *Interaction, growth, and*
642 *ordering of epitaxial graphene on SiC {0001} surfaces: A comparative photoelectron*
643 *spectroscopy study.* J Physical review B, 2008. **77**(15): p. 155303.

644 48. Ridene, M., J.C. Girard, L. Travers, C. David, and A. Ouerghi, *STM/STS investigation*
645 *of edge structure in epitaxial graphene.* Surface Science, 2012. **606**(15): p. 1289-
646 1292.
647 49. Rollings, E., G.H. Gweon, S.Y. Zhou, B.S. Mun, J.L. McChesney, B.S. Hussain, A.V.
648 Fedorov, P.N. First, W.A. de Heer, and A. Lanzara, *Synthesis and characterization of*
649 *atomically thin graphite films on a silicon carbide substrate.* Journal of Physics and
650 Chemistry of Solids, 2006. **67**(9): p. 2172-2177.
651 50. Tanuma, S., C.J. Powell, and D.R. Penn, *Calculation of electron inelastic mean free*
652 *paths (IMFPs) VII. Reliability of the TPP-2M IMFP predictive equation.* 2003. **35**(3):
653 p. 268-275.
654 51. Giusca, C.E., S.J. Spencer, A.G. Shard, R. Yakimova, and O. Kazakova, *Exploring*
655 *graphene formation on the C-terminated face of SiC by structural, chemical and*
656 *electrical methods.* Carbon, 2014. **69**: p. 221-229.
657 52. Sun, G.F., Y. Liu, S.H. Rhim, J.F. Jia, Q.K. Xue, M. Weinert, and L. Li, *Si diffusion*
658 *path for pit-free graphene growth on SiC(0001).* Physical Review B, 2011. **84**(19): p.
659 195455.
660 53. Zarotti, F., B. Gupta, F. Iacopi, A. Sgarlata, M. Tomellini, and N. Motta, *Time*
661 *evolution of graphene growth on SiC as a function of annealing temperature.* J
662 Carbon, 2016. **98**: p. 307-312.
663 54. Gupta, B., M. Notarianni, N. Mishra, M. Shafiei, F. Iacopi, and N. Motta, *Evolution of*
664 *epitaxial graphene layers on 3C SiC/Si (1 1 1) as a function of annealing temperature*
665 *in UHV.* J Carbon, 2014. **68**: p. 563-572.
666 55. Yazdi, G.R., T. Iakimov, and R. Yakimova, *Epitaxial Graphene on SiC: A Review of*
667 *Growth and Characterization.* 2016. **6**(5): p. 53.
668 56. Dimitrakopoulos, C., Y.-M. Lin, A. Grill, D.B. Farmer, M. Freitag, Y. Sun, S.-J. Han,
669 Z. Chen, K.A. Jenkins, Y. Zhu, Z. Liu, T.J. McArdle, J.A. Ott, R. Wisnieff, and P.
670 Avouris, *Wafer-scale epitaxial graphene growth on the Si-face of hexagonal SiC*
671 *(0001) for high frequency transistors.* 2010. **28**(5): p. 985-992.
672 57. Real, M.A., E.A. Lass, F.-H. Liu, T. Shen, G.R. Jones, J.A. Soons, D.B. Newell, A.V.
673 Davydov, R.E. Elmquist, and Measurement, *Graphene epitaxial growth on SiC*
674 *(0001) for resistance standards.* J IEEE Transactions on Instrumentation, 2013. **62**(6):
675 p. 1454-1460.
676 58. Vesapuisto, E., W. Kim, S. Novikov, H. Lipsanen, and P. Kuivalainen, *Growth*
677 *temperature dependence of the electrical and structural properties of epitaxial*
678 *graphene on SiC(0001).* 2011. **248**(8): p. 1908-1914.
679 59. Hu, T., H. Bao, S. Liu, X. Liu, D. Ma, F. Ma, and K. Xu, *Near-free-standing epitaxial*
680 *graphene on rough SiC substrate by flash annealing at high temperature.* Carbon,
681 2017. **120**: p. 219-225.
682 60. Hannon, J.B. and R.M. Tromp, *Pit formation during graphene synthesis on*
683 *SiC(0001): In situ electron microscopy.* Physical Review B, 2008. **77**(24): p. 241404.
684 61. Dimitrakopoulos, C., A. Grill, T. McArdle, Z. Liu, R. Wisnieff, and D. Antoniadis,
685 *Effect of SiC Wafer Miscut Angle on the Morphology and Hall Mobility of Epitaxially*
686 *Grown Graphene.* Applied Physics Letters, 2011. **98**: p. 222105.
687 62. Borovikov, V. and A. Zangwill, *Step-edge instability during epitaxial growth of*
688 *graphene from SiC(0001).* Physical Review B, 2009. **80**(12): p. 121406.
689 63. Bolen, M.L., S.E. Harrison, L.B. Biedermann, and M.A. Capano, *Graphene formation*
690 *mechanisms on $4H\text{-SiC}(0001)$.* Physical Review B, 2009. **80**(11): p. 115433.
691 64. Starke, U. and C. Riedl, *Epitaxial graphene on SiC (0001) and: from surface*
692 *reconstructions to carbon electronics.* J Journal of Physics: Condensed Matter, 2009.
693 **21**(13): p. 134016.

694 65. Ouerghi, A., M. Marangolo, R. Belkhou, S. El Moussaoui, M. Silly, M. Eddrief, L.
695 Largeau, M. Portail, B. Fain, and F. Sirotti, *Epitaxial graphene on 3C-SiC (111)*
696 *pseudosubstrate: Structural and electronic properties.* J Physical review B, 2010.
697 **82**(12): p. 125445.
698 66. Lee, D.S., C. Riedl, B. Krauss, K. von Klitzing, U. Starke, and J.H. Smet, *Raman*
699 *spectra of epitaxial graphene on SiC and of epitaxial graphene transferred to SiO2.* J
700 Nano letters, 2008. **8**(12): p. 4320-4325.
701 67. Röhrl, J., M. Hundhausen, K. Emtsev, T. Seyller, R. Graupner, and L. Ley, *Raman*
702 *spectra of epitaxial graphene on SiC (0001).* J Applied Physics Letters, 2008. **92**(20):
703 p. 201918.
704 68. Daas, B.K., S.U. Omar, S. Shetu, K.M. Daniels, S. Ma, T.S. Sudarshan, and M.V.S.
705 Chandrashekhar, *Comparison of Epitaxial Graphene Growth on Polar and Nonpolar*
706 *6H-SiC Faces: On the Growth of Multilayer Films.* Crystal Growth & Design, 2012.
707 **12**(7): p. 3379-3387.
708 69. Liu, Z., Z. Su, Q. Li, L. Sun, X. Zhang, Z. Yang, X. Liu, Y. Li, Y. Li, and F.J.R.a. Yu,
709 *Induced growth of quasi-free-standing graphene on SiC substrates.* 2019. **9**(55): p.
710 32226-32231.
711 70. Yager, T., A. Lartsev, S. Mahashabde, S. Charpentier, D. Davidovikj, A. Danilov, R.
712 Yakimova, V. Panchal, O. Kazakova, A. Tzalenchuk, S. Lara-Avila, and S. Kubatkin,
713 *Express Optical Analysis of Epitaxial Graphene on SiC: Impact of Morphology on*
714 *Quantum Transport.* Nano Letters, 2013. **13**(9): p. 4217-4223.
715 71. Yazdi, G.R., R. Vasiliauskas, T. Iakimov, A. Zakharov, M. Syväjärvi, and R.
716 Yakimova, *Growth of large area monolayer graphene on 3C-SiC and a comparison*
717 *with other SiC polytypes.* Carbon, 2013. **57**: p. 477-484.

718

719 ## Supporting information

720 The atomic concentration of graphene and SiC components of high resolution C1s XPS
721 (Figure S1) and the calculated number of graphene layers at various annealing temperature
722 and growth time by standard technique are tabulated in Table 1 for on-axis and off-axis SiC.
723 The components at ~283 eV and 284.6 eV correspond to the SiC and graphene respectively.
724 The low intensity peaks at 284.8 eV and 285.2 eV belong to the covalently bonded carbons to
725 the SiC (S1) and carbons having sp^2 configuration(S2) in buffer layer [69].

726

727 **Table S 1: Calculated number of graphene layers in standard method.** The atomic concentration of SiC and
728 graphene components of C1s XPS core level spectra and the number of graphene layers calculated accordingly

for epitaxial graphene grown by standard method at different growth temperatures and time on on-axis and off-axis SiC.

On-axis SiC						Off-axis SiC					
T (˚C)	Growth time (mins)	Atomic concentration (%)		Graphene layers	Error ±	T (˚C)	Growth time (mins)	Atomic concentration (%)		Graphene layers	Error ±
		SiC	Graphene					SiC	Graphene		
1280	1	29.55	63.71	3.87	0.40	1280	1	40.13	53.06	2.69	1.77
1300	1	23.67	71.46	4.87	0.48	1300	1	34.38	59.29	3.29	0.49
	2	18.18	76.00	5.97	0.48	1350	15	5.68	86.17	11.52	0.62

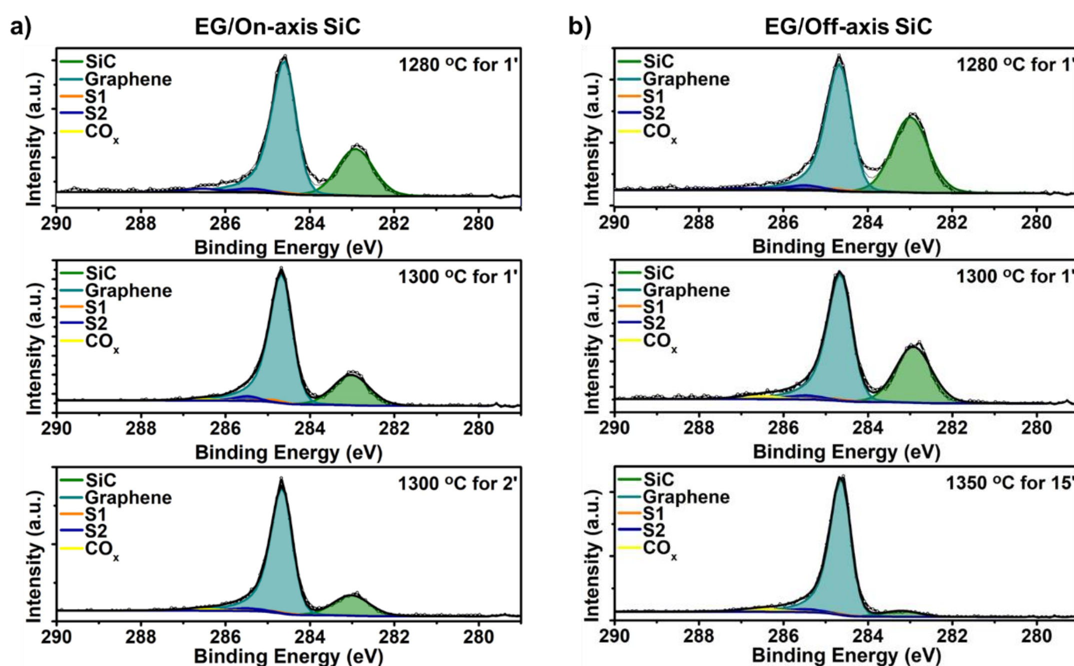

Figure S 1: Chemical characterization of epitaxial graphene grown by standard method. The C1s XPS core level spectra for growth of epitaxial graphene by standard method at different growth temperatures and time on (a) on-axis and (b) off-axis SiC.

Figure S2 shows the STM image of epitaxial graphene grown on on-axis SiC and off-axis SiC by annealing at 1300 C for 1 minute using standard technique. The noncontinuous islands of epitaxial graphene on on-axis SiC in Figure S2a show wrinkles and pits on the surface. The line profile along the red line indicated on Figure S2b shows narrow terraces of

739 up to 10 nm for epitaxial graphene grown on off-axis SiC. The steps of epitaxial graphene are
740 covered with small wrinkles.

741 Figure S3 and S4 shows the morphology of the epitaxial graphene grown on on-axis and off-
742 axis SiC by FTF technique at different annealing temperatures and growth times. The
743 optimum growth condition for FTF growth on on-axis SiC and off-axis SiC is 1300 ˚C for 15
744 minutes and 1350 ˚C for 10 minutes respectively. The epitaxial graphene grown at these
745 conditions are led to the surface with the most uniform wide terraces of up to 5µm on on-axis
746 SiC and 440 nm width on off-axis SiC. The FTF technique is improved the morphology and
747 the terrace size of the epitaxial graphene grown on both on-axis and off-axis SiC by
748 decreasing the growth rate owing to the controlled sublimation of Si from the surface.

749

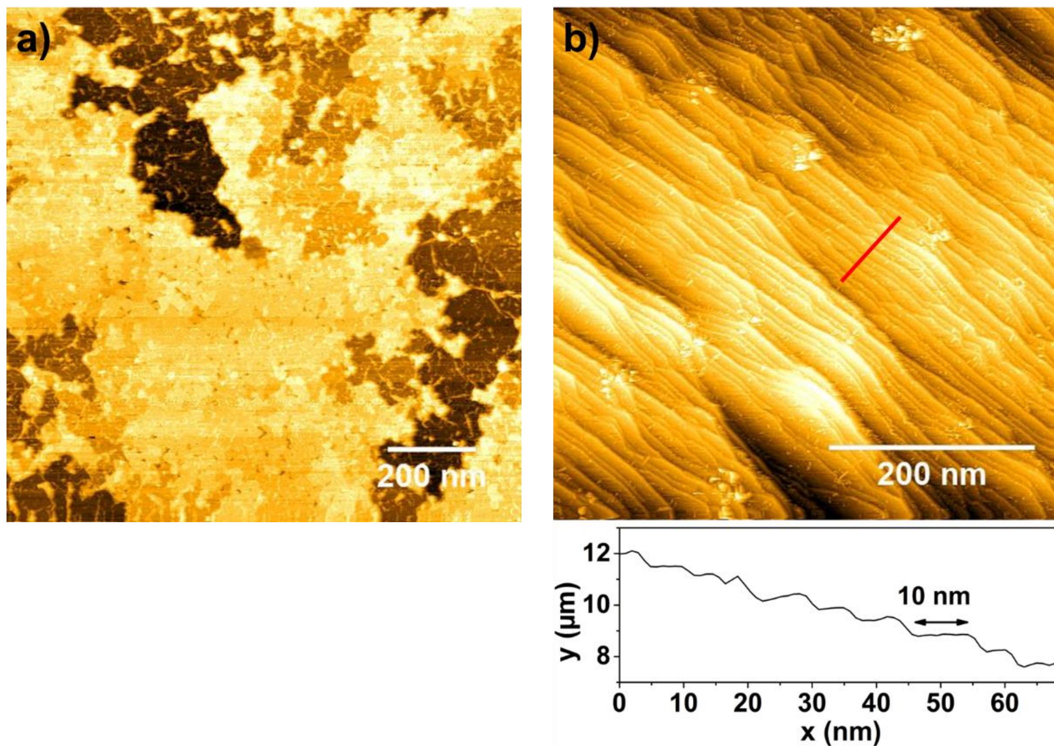

750 **Figure S 2: Morphology analysis of epitaxial graphene grown by standard method.** The in-situ STM image
751 of epitaxial graphene on (a) on-axis SiC (U= -0.5 V; I= 0.1 nA) (b) off-axis SiC (U= - 1.5 V; I= 0.8 nA) grown
752 at 1300 ˚C for 1 minute.

753

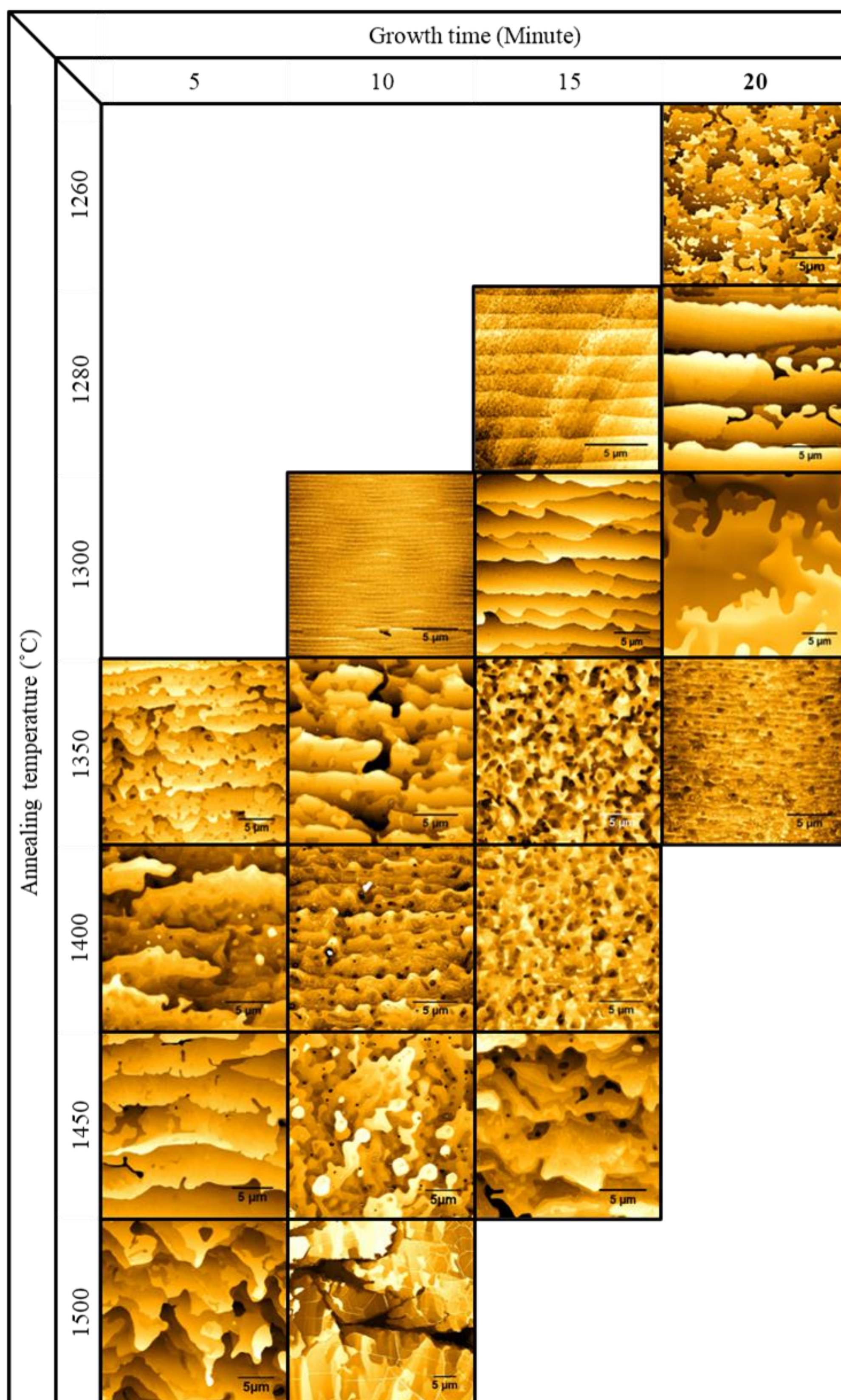

754 **Figure S 3. Morphology analysis of epitaxial graphene grown by FTF method on on-axis SiC.** The AFM

755 library of epitaxial graphene grown on on-axis SiC by FTF technique at various growth temperature and growth

756 time.

757

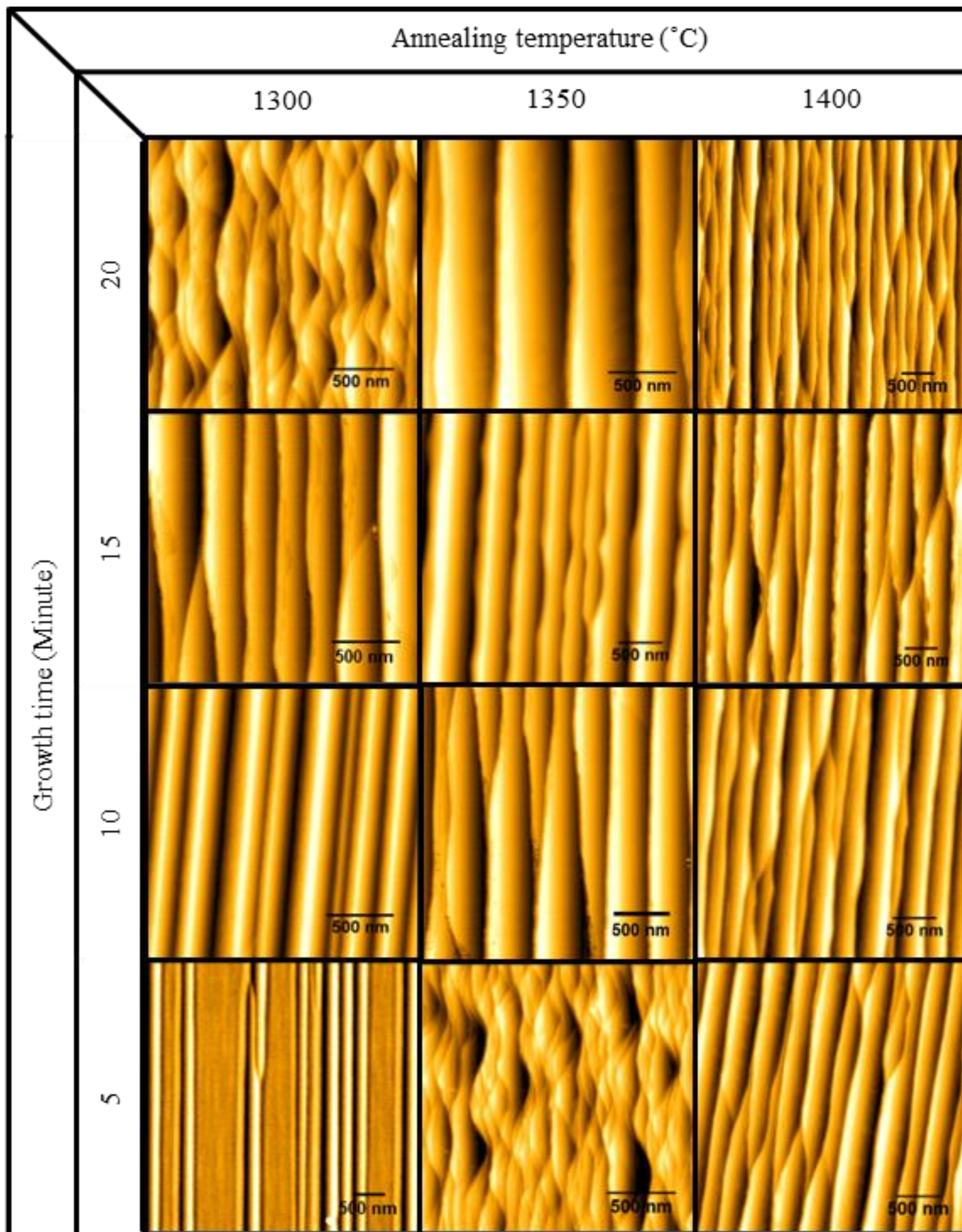

758 **Figure S 4. Morphology analysis of epitaxial graphene grown by FTF method on off-axis SiC.** The AFM

759 library of epitaxial graphene grown on on-axis SiC by FTF technique at various growth temperature and growth

760 time.

761

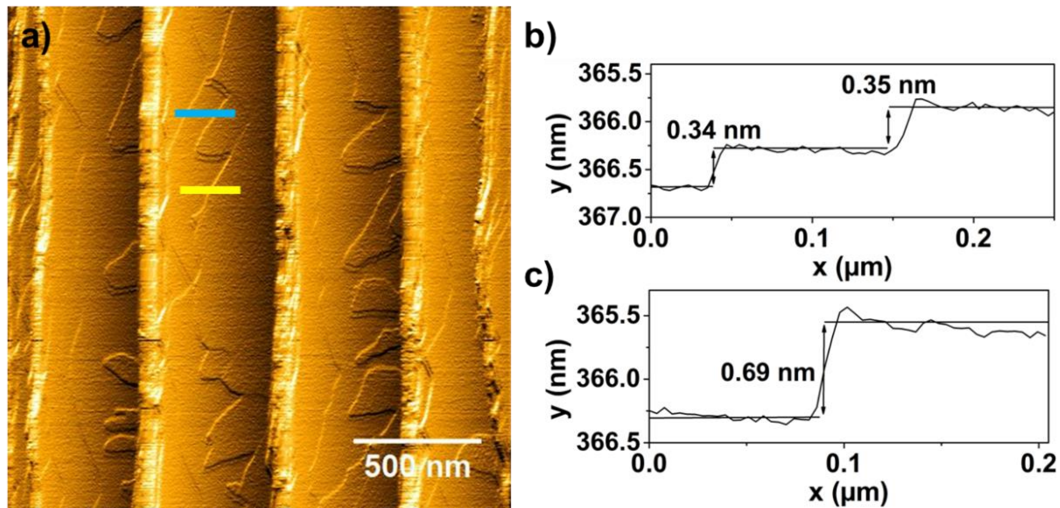

762 **Figure S 5.** (a) The shade corrected AFM image of epitaxial graphene grown at 1350 ˚C for 20 minutes. The
763 line profile along the (b) blue and (c) yellow lines as indicated on (a) showing monolayer and bilayer graphene
764 islands on the epitaxial graphene steps respectively.

765 Figure S5a shows the shade corrected AFM image of the epitaxial graphene grown at 1350
766 ˚C for 20 minutes. The presence of monolayer and bilayer graphene islands can be clearly
767 seen in S5(a) and the line profile along the blue and yellow lines proves the monolayer and
768 bilayer graphene thickness of 0.34 nm and 0.69 nm respectively.

769 Figure S6 shows tapping mode AFM and KPFM images of a partially graphitised on-axis SiC
770 surface prepared by face-to-face annealing at 1300 °C for 5 minutes. Figure S7 shows the
771 plots of the line profiles taken along an identical path from each channel, corresponding to
772 the black, blue and red paths in Figure S6 (a)-(c). While variations in the graphene layer
773 thickness are unclear in the height channel (Figure S6(a)), the contact potential difference
774 (CPD) in Figure S1(c) clearly shows three contrast levels which correspond to the SiC
775 substrate (low CPD), monolayer graphene, and bilayer or multilayer graphene (high CPD)
776 [70]. The phase contrast in Figure S6(b) shows clear differences between graphene and SiC
777 region, though the regions of bilayer/multilayer graphene are not clear. From the line profiles
778 in Figure S7 is can be seen that the graphene regions extend from the step edges of the SiC

779 substrate, and multilayer graphene is formed at taller, step-bunched SiC step edges. This is

780 consistent with previous observations of graphene formation on SiC substrates [71].

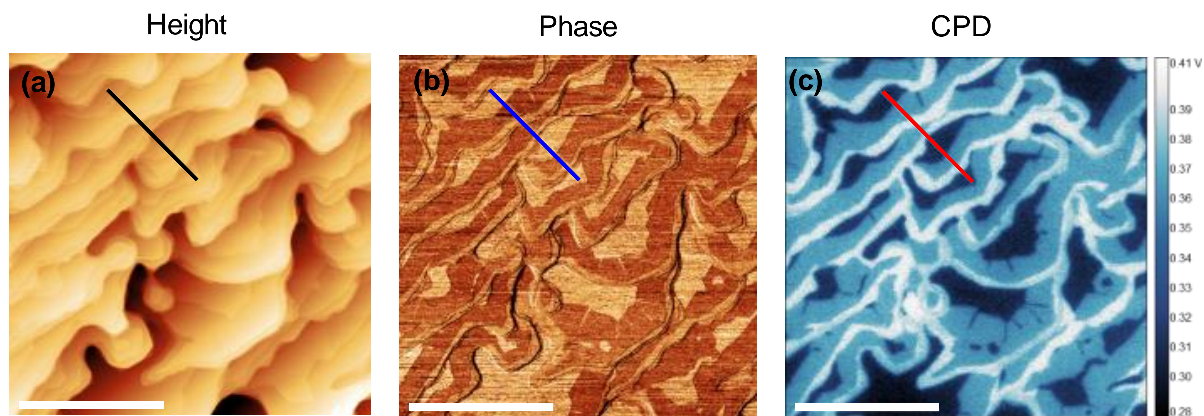

781

782 **Figure S 6:** KPFM measurements of a partially graphitised SiC surface. (a) and (b) show the height and phase

783 channels, respectively, acquired from the first pass, and (c) shows the contact potential difference (CPD)

784 measured on the second pass. Scale bars for all images are 4 µm.

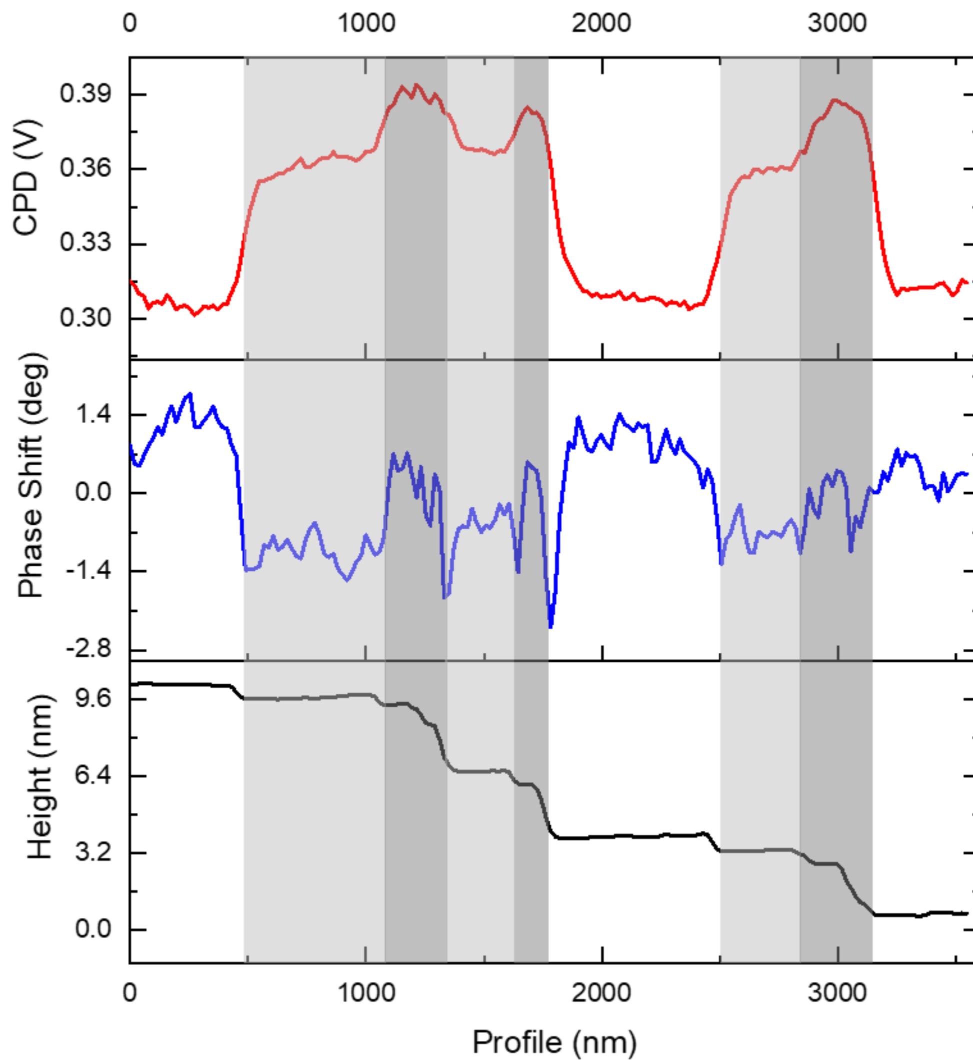

785

786 **Figure S 7:** Line profiles measured along the black, blue and red paths drawn in Figure S1. All

787 the profiles correspond to the same path from the three different channels. Regions of

788 monolayer graphene are shaded in light grey, and bilayer/multilayer graphene is shaded in

789 dark grey. Unshaded regions correspond to the SiC substrate.

790

791

792

793 Figure S8 shows the analysis of the various components of the FFT transform shown in

794 Figure 7c and 7d. The back Fourier Transform of the central, middle and outermost hexagons

795 as marked in the FFT inset images of Figure S8 provide the real space image of the moiré

796 pattern, second nearest neighbour and first nearest neighbour atoms respectively.

797

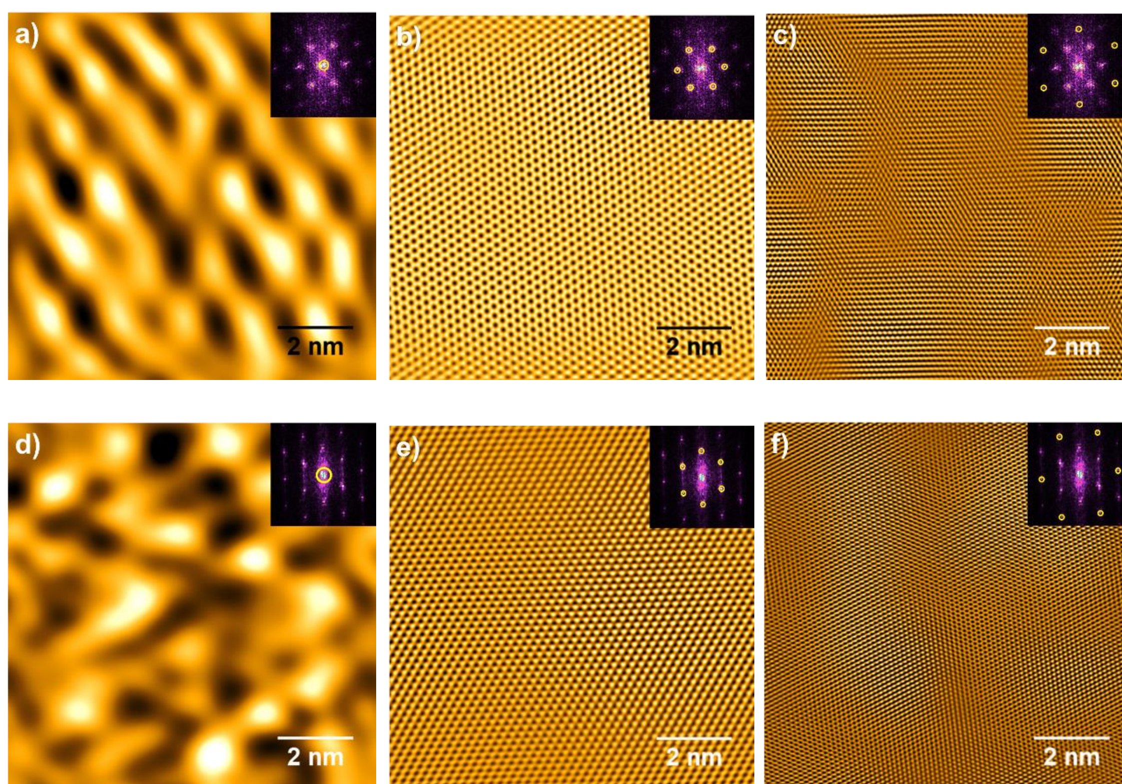

798 **Figure S 8. Structural analysis of FTF grown epitaxial graphene.** The Fourier components of the epitaxial

799 graphene grown on (a-c) on-axis SiC and (d-f) off-axis SiC by FTF technique. The insets are the FFT images

800 and the marked central, middle and outermost hexagon indicate (a,d) the Moiré pattern, (b,e) second nearest

801 neighbour and (c,f) the first nearest neighbour graphene atoms of the Fourier incorporators respectively.

802

803

804

805 The Raman spectra of FTF grown epitaxial graphene on on-axis SiC and off-axis SiC at

806 optimised growth conditions of annealing at 1300 ˚C for 15 mins and 1350 ˚C for 10 minutes

807 and the epitaxial graphene grown on on-axis SiC and off-axis SiC at 1300 ˚C for 1 minute by

808 standard method are shown in Figure S9. The G peak for all the samples is at 1606 cm^{-1} and

809 the position of D peak is around 1367 cm^{-1}. The intensity of samples grown by standard

810 technique shown higher intensity D peaks in comparison to the FTF grown samples. This

811 confirms the defective epitaxial graphene grown in standard technique and how the FTF

812 method is improved the quality of epitaxial graphene.

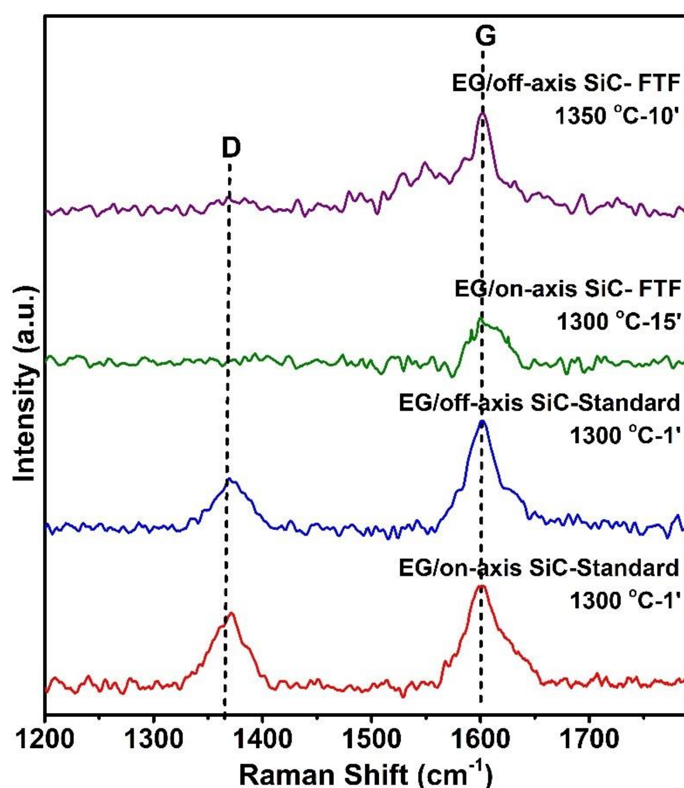

813

814 **Figure S 9: Raman characterization of epitaxial graphene grown by FTF and standard technique.** The

815 comparison of Raman spectra around the D and G peaks for epitaxial graphene grown by FTF technique on on-

816 axis and off-axis SiC at optimised growth conditions of annealing at 1300 ˚C for 15 mins and 1350 ˚C for 10

817 minutes and epitaxial graphene grown by standard technique on on-axis and off-axis SiC by annealing at 1300

818 ˚C for 1 minute. The bare SiC Raman spectra is partial subtraction as background from all the spectra.

819